CONFIDENTIAL

Copy
RM L55L19

NACA RM L55L19

NACA

CASE FILE
COPY

RESEARCH MEMORANDUM

TRANSONIC WIND-TUNNEL MEASUREMENTS OF STATIC LATERAL AND DIRECTIONAL STABILITY AND VERTICAL-TAIL LOADS FOR A MODEL WITH A 45° SWEPTBACK WING

By Joseph M. Hallissy, Jr.

Langley Aeronautical Laboratory
Langley Field, Va.

CLASSIFICATION CHANGED TO UNCLASSIFIED

AUTHORITY: NASA TECHNICAL PUBLICATIONS ANNOUNCEMENTS NO. 29

EFFECTIVE DATE: AUGUST 19, 1960 WHL

CLASSIFIED DOCUMENT

This material contains information affecting the National Defense of the United States within the meaning of the espionage laws, Title 18, U.S.C., Secs. 793 and 794, the transmission or revelation of which in any manner to an unauthorized person is prohibited by law.

NATIONAL ADVISORY COMMITTEE
FOR AERONAUTICS

WASHINGTON

May 17, 1956

CONFIDENTIAL

NATIONAL ADVISORY COMMITTEE FOR AERONAUTICS

RESEARCH MEMORANDUM

TRANSONIC WIND-TUNNEL MEASUREMENTS OF STATIC LATERAL AND DIRECTIONAL STABILITY AND VERTICAL-TAIL LOADS FOR A MODEL WITH A 45° SWEPTBACK WING

By Joseph M. Hallissy, Jr.

SUMMARY

An investigation to determine the vertical-tail loads and airplane characteristics in sideslip for a model of a swept-wing fighter-type airplane was conducted in the Langley 16-foot transonic tunnel at Mach numbers from 0.80 to 1.03 and at angles of attack to 15°. The wing had 45° sweepback, an aspect ratio of 3.56, a taper ratio of 0.30, and utilized NACA 64A007 airfoil sections.

The directional stability at a Mach number of 0.80 was approximately constant through the test angle-of-attack range. At higher speeds, although having a greater initial value than at a Mach number of 0.80, the directional stability decreased with angle of attack, as did the vertical-tail loads. At subsonic speeds the directional stability for zero angle of attack was found to be somewhat less at very small angles of sideslip than at moderate angles. The load on the exposed vertical tail represented between 60 and 80 percent of the total tail contribution to side force, and the maximum travel of the center of pressure with angle of attack and Mach number was about 7 percent of the height upward and 14 percent of the chord rearward.

INTRODUCTION

Many of the trends in the design of present-day fighter aircraft have increased the problems of providing adequate lateral and directional stability and of properly estimating tail loads. This is particularly so since the usual operating range of such aircraft now includes subsonic, transonic, and supersonic flight and an extended angle-of-attack range. Reference 1 discusses in detail some of these stability problems, while reference 2 considers the problem of tail-loads estimation. Both of these references point to the necessity, in the present state of design ability, of adequate wind-tunnel studies in the development of specific designs.

Therefore, when a supersonic-fighter design was investigated in the Langley 16-foot tunnel recently, the test program included studies of lateral and directional stability and of vertical-tail loads. This paper presents the results of this part of the investigation. Previously reported are the longitudinal stability and performance data obtained in the same program (references 3, 4, and 5). Data are presented in this report for Mach numbers from 0.80 to 1.03, angles of attack from 0° to 15°, and sideslip angles generally to 5°.

SYMBOLS

The center-of-gravity location is shown in figure 1. All coefficients, including the tail-load coefficients, are referred to this center-of-gravity location through the stability axes system.

b wing span

b_t vertical-tail height from defined root chord, figure 2

$\bar{c}$ wing mean aerodynamic chord

c_t local vertical-tail chord

C_l rolling-moment coefficient, $\frac{\text{Rolling moment}}{qSb}$

C_{l_t} rolling-moment coefficient due to load on the exposed vertical tail, $\frac{\text{Tail rolling moment}}{qSb}$

C_m pitching-moment coefficient, $\frac{\text{Pitching moment}}{qS\bar{c}}$

C_n yawing-moment coefficient, $\frac{\text{Yawing moment}}{qSb}$

C_{n_t} yawing-moment coefficient due to load on the exposed vertical tail, $\frac{\text{Tail yawing moment}}{qSb}$

C_Y side-force coefficient, $\frac{\text{Side force}}{qS}$

C_{Y_t} side-force coefficient due to load on the exposed vertical tail, $\frac{\text{Tail side force}}{qS}$

M free-stream Mach number

q free-stream dynamic pressure

S total wing area

α angle of attack measured from the wing chord plane, deg

β angle of sideslip, deg

Stability derivatives:

$$C_{l_\beta} = 57.3 \frac{C_{l_{(\beta=5^\circ)}} - C_{l_{(\beta=0^\circ)}}}{5}$$

$$C_{n_\beta} = 57.3 \frac{C_{n_{(\beta=5^\circ)}} - C_{n_{(\beta=0^\circ)}}}{5}$$

$$C_{Y_\beta} = 57.3 \frac{C_{Y_{(\beta=5^\circ)}} - C_{Y_{(\beta=0^\circ)}}}{5}$$

$$C_{l_{t_\beta}} = 57.3 \frac{C_{l_{t_{(\beta=5^\circ)}}} - C_{l_{t_{(\beta=0^\circ)}}}}{5}$$

$$C_{n_{t_\beta}} = 57.3 \frac{C_{n_{t_{(\beta=5^\circ)}}} - C_{n_{t_{(\beta=0^\circ)}}}}{5}$$

$$C_{Y_{t_\beta}} = 57.3 \frac{C_{Y_{t_{(\beta=5^\circ)}}} - C_{Y_{t_{(\beta=0^\circ)}}}}{5}$$

APPARATUS AND TUNNEL

Tunnel and Model Support

These tests were conducted in the Langley 16-foot transonic tunnel which has a slotted throat of octagonal cross section.

The model was supported with a sting which was mounted on a strut passing through the tunnel floor. The strut moved on the arc of a circle to provide angle-of-attack variation without moving the model center of gravity from the tunnel center line. Data obtained at a fixed sideslip angle of 5° were obtained by means of a bent coupling in the sting. Variable sideslip data at zero angle of attack were obtained by rolling the model 90° and operating the strut as for angle of attack.

Model

Figure 1 is a three-view sketch of the model. Vertical-tail geometry and the principal dimensions of the wing and horizontal tail are given in figure 2. A photograph of the complete model installed in the test section of the tunnel is given as figure 3.

Force and moment measurements on the model were obtained using two internal strain-gage balances. The main balance measured the six components of the complete model, and a smaller three-component balance located at the base of the vertical tail measured the side force and bending and twisting moments on the exposed part of the vertical tail. Figure 4 is a cross-sectional sketch through the lower part of the vertical tail which shows the three-component-balance installation. No seals were installed, and cross flow was, therefore, possible through the clearance gaps and under the vertical tail ahead and behind the balance-gage beams. An alternate tail (having no balance or clearance gaps) was also available and was used for some runs.

Some tests were made with the wing equipped with a longitudinal stability "fix" consisting of 6° leading-edge droop from 0.25 to 0.71 semispan and 15-percent chord-extensions drooped 6° from 0.71 to 1.00 semispan. This fix is one of several investigated in the longitudinal tests on this model, and is described in more detail in reference 4.

TESTS

The test Reynolds number based on wing mean aerodynamic chord varied between about 6.0×10^6 and 7.2×10^6. For all tests the horizontal tail was installed and set at zero incidence (parallel to the wing chord plane). Test Mach numbers were 0.80, 0.90, 0.95, 1.00, and 1.03, although for the last two of these, data were not obtained at the highest angles of attack due to support-system limitations. The other variables and the configurations tested are indicated in the following table:

Wing	Vertical tail	α, deg	β, deg	Data presented	Figures
Basic	Plain (sealed)	0	-5 to 5	C_l, C_n, C_Y	5
				C_{l_β}, C_{n_β}, C_{Y_β}	6
				C_m	15(a)
Basic	Instrumented (unsealed)	0	-5 to 5	C_l, C_n, C_Y	5
				C_{l_β}, C_{n_β}, C_{Y_β}	6
				C_m	15(a')
				C_{l_t}, C_{n_t}, C_{Y_t}	8
Basic	Off	0	-5 to 15	C_l, C_n, C_Y	7
				C_m	15(b)
Basic	Instrumented (unsealed)	0 to 15	0, 5	C_{l_β}, C_{n_β}, C_{Y_β}	9, 10
				ΔC_m	16
				$C_{l_{t_\beta}}$, $C_{n_{t_\beta}}$, $C_{Y_{t_\beta}}$	11, 12
				Vertical-tail center of pressure	13
Basic	Off	0 to 15	0, 5	C_{l_β}, C_{n_β}, C_{Y_β}	9, 10
				ΔC_m	16
Fixes on	Instrumented (unsealed)	0 to 15	0, 5	C_{l_β}, C_{n_β}, C_{Y_β}	14
				$C_{l_{t_\beta}}$, $C_{n_{t_\beta}}$, $C_{Y_{t_\beta}}$	14

Data obtained in angle-of-attack tests at constant sideslip angles of 0° and 5° have been reduced directly to the sideslip derivatives and are presented in this form throughout the report.

RESULTS AND DISCUSSION

Effect of the Unsealed Vertical-Tail Root on Airplane Coefficients

It was believed at the time of the tests that the small gap around the base of the vertical tail could be left unsealed without adverse effects, and therefore, as indicated in the table of tests, most of the tests were made with no seal. The results, however, as shown in figures 5 and 6, indicate effects of appreciable magnitude. Figure 5 shows that at $\alpha = 0^\circ$ the lack of a seal resulted in decreased (absolute) values of all three lateral coefficients, and thus in the three sideslip derivatives. This was especially true for small angles of sideslip, the curves for the instrumented (unsealed) tail being appreciably more flattened as they pass through $\beta = 0^\circ$.

The lateral derivatives as determined from the end points only ($+5^\circ$ and -5°) are shown in figure 6 for the two tail installations. The loss caused by the unsealed root gap is as much as 20 percent for C_{n_β} and 50 percent for C_{l_β}. For all three of these derivatives the gap has little effect on the variations which occur with Mach number, and it is believed that qualitatively the tail loads and tail-effectiveness information obtained is sound, although some quantitative error has been introduced by the lack of seals.

Directional and Lateral Stability

Effect of sideslip at $\alpha = 0^\circ$.- In making the variable sideslip tests, many points were taken near $\beta = 0^\circ$, in anticipation of a possible loss of stability for small angles of sideslip. Both C_n and C_Y for the tail-on case do show slope reductions near $\beta = 0^\circ$ for some Mach numbers (fig. 5). The slope of C_n with β, for example, is reduced 15 to 20 percent (plain tail) for Mach numbers from 0.80 to 0.95, but none at Mach number 1.00 or 1.03. Most of this reduction in slope is chargeable to the tail itself, as is indicated by the vertical-tail-load data of figure 8, and is probably due to being in the wake of the fuselage and canopy. Some of the slope reduction for small sideslip angles also comes from the wing-body combination as shown by the tail-off data of figure 7. This, of course, stems from the tendency for both the force and moment on bodies alone to be nonlinear with angle of inclination. (As an example, see the body data of ref. 6.)

For Mach number 0.95 and higher, the tail-on data, particularly C_n in figure 5(b) show a number of nonlinearities which are generally similar for both the sealed and unsealed case and which are symmetric about $\beta = 0^\circ$. These nonlinearities evidently come from the load on

the tail itself, since they are also found in the tail-load curves of figure 8 and are not found in the tail-off data of figure 7. Considering that they do not occur for $M = 0.80$ and 0.90, these nonlinearities are probably related to such local flow field conditions as horizontal-tail shock waves.

Sideslip derivatives at angle of attack.- In addition to the airplane tail-on and tail-off sideslip derivatives which are shown as functions of angle of attack (fig. 9) and Mach number (fig. 10), the total vertical-tail contribution has been computed and is given in figures 11 and 12. These were obtained by subtracting the vertical tail-off derivatives from the tail-on derivatives.

The side-force derivative C_{Y_β} for the vertical tail-off condition generally increases in absolute value both with angle of attack (fig. 9) and with Mach number (fig. 10). For the tail-on condition, however, C_{Y_β} decreases with α, indicating reductions in tail contribution (as shown in fig. 11) at high angles of attack, particularly at the higher Mach numbers. These characteristics of the tail contribution to C_Y are reflected in the C_n data which show similar characteristics. The directional stability C_{n_β} for the complete airplane is approximately constant throughout the angle-of-attack range (0° to 15°) for a Mach number of 0.8, figure 9. At higher speeds (Mach number 0.95 to 1.03), although having a greater initial value than at $M = 0.80$, C_{n_β} decreased with angle of attack (but did not fall below the $M = 0.8$ level in the range of these tests). The tail contribution to C_{n_β}, figure 11, shows similar characteristics.

The rolling moment due to sideslip C_{l_β}, has a variation with angle of attack, figure 9, which is typical for swept-wing airplanes. It is due to the lift-curve variations and changes in stalling characteristics which occur with changes in effective sweep angle in the sideslipping condition. The effect of increasing Mach number is to reduce the nonlinearities of these curves. Similar results for other swept-wing configurations are shown in reference 7. The effect of adding the vertical tail is to make the zero angle-of-attack values of C_{l_β} negative, but at high angles of attack this negative contribution is decreased or becomes positive.

Vertical-Tail Loads

All of the vertical-tail loads and moments obtained in this investigation have been reduced to coefficient form using airplane dimensions and the stability-axes system so as to be directly comparable to the other coefficients presented in the report. Variations of the tail loads and moments with sideslip angle at zero angle of attack are given in figure 8, while the variations of the tail derivatives with angle of attack and Mach number obtained from data taken at 5° sideslip angle have been included in figures 11 and 12 with the total vertical-tail contributions to lateral and directional stability. The latter, of course, include not only the loads on the vertical tail but also the loads induced by the vertical tail on the fuselage and other parts of the airplane.

As with the total tail contributions ΔC_{Y_β} and ΔC_{n_β}, both $C_{Y_{t_\beta}}$ and $C_{n_{t_\beta}}$ decrease with angle of attack, especially at the higher speeds (fig. 11). Both ΔC_{Y_β} and ΔC_{n_β} have larger absolute values than $C_{Y_{t_\beta}}$ and $C_{n_{t_\beta}}$, indicating that for low angles of attack about 30 percent of the total tail contribution is from load carried on the fuselage. These total increments, however, decrease more rapidly with angle of attack than the tail loads, so that at the higher angles the load carried on the fuselage is of the order of 20 percent of the total tail contribution.

The value of ΔC_{l_β} is for all conditions less negative (or more positive) than $C_{l_{t_\beta}}$, figure 11. This is due to the fact that the load on the vertical tail induces an asymmetric loading on the horizontal tail such as to cause a significant rolling-moment contribution opposite in sign to that produced by the vertical-tail loading. Similar results have been shown in reference 8 which reports loading measurements made on a tail-assembly—body configuration.

Both $C_{l_{t_\beta}}$ and ΔC_{l_β} decrease more rapidly with angle of attack than the other derivatives, which is the direct result of the use of the stability axes system.

The variations of measured tail load with Mach number (fig. 12) in the speed range of the present tests are relatively small and generally follow the trend of total tail contribution.

The center-of-pressure locations for the exposed vertical tail as determined directly from vertical-tail moments and lateral forces are shown in figures 13(a) and (b). They show a generally rearward and outward trend with both angle of attack (fig. 13(a)) and Mach number

(fig. 13(b)). For all test conditions the center of pressure was located between 0.45 and 0.52 b_t, and between 0.18 and 0.32 c_t. The symbols of figure 13(a) are actual test points, while those of figure 13(b) are cross plotted from the curves of 13(a). In utilizing these data, it should be kept in mind that they were obtained without seals at the tail root. Leakage due to lack of seals may have unloaded the inboard sections of the vertical tail with a resultant outboard movement of the center of pressure.

Effect of Leading-Edge Chord-Extensions on Lateral and Directional Characteristics and on Tail Loads

Tests with the longitudinal stability "fix" installed were made through an angle-of-attack range at sideslip angles of 0° and 5°. Results are shown in figure 14.

In earlier tests this fix was found to improve the longitudinal characteristics, although not extensively (see ref. 4). Since the chord-extension affects the longitudinal characteristics by preventing or reducing the tip stall, it was anticipated that the effect on the rolling moment in sideslip tests would be appreciable. This was found to be the case. The linear portion of the C_{l_β} curve with α is generally extended and the upward breaks are less severe with the fixes installed, indicating that the left and right wing lift curves are more consistent; that is, the separation is better controlled and more gradual so that the erratic breaks in the curve caused by abrupt stalling of one wing are reduced.

The effects of the fix on C_{n_β} and C_{Y_β} were generally small. The tail loads, as measured with the tail balance and shown on the right side of figure 14 are also little affected by the addition of the fix, indicating that the effect of the fix is confined to the wing, as would be expected.

Pitching Moments in Sideslip

Figure 15(a) indicates that only a very small nose-down increment in pitching-moment coefficient (less than 0.005) occurs with this model at 5° sideslip at zero angle of attack. Tests to higher sideslip angles with the vertical tail off (fig. 15(b)) show a more severe nose-down tendency developing as the sideslip exceeds 10°. This tendency probably would also occur with the vertical tail on, but this is not certain since the presence of the vertical tail may appreciably alter conditions on the horizontal tail and hence the pitching moment.

Figure 16 indicates that the variations with angle of attack for the increment in pitching-moment coefficient due to 5° sideslip was rather nonlinear, especially above an angle of about 8°. Values as large as 0.015 were measured compared to less than 0.005 at zero angle of attack.

CONCLUSIONS

A transonic wind-tunnel investigation has been made on a model of a swept-wing fighter-type airplane to determine airplane characteristics and vertical-tail loads in sideslip. Although the vertical-tail-fuselage juncture was not sealed for most of the tests (thus introducing some quantitative errors), the following conclusions are indicated:

1. At zero angle of attack where variable sideslip tests were made, C_{n_β} was 15 to 20 percent less for Mach numbers of 0.80 to 0.95 for the very small sideslip angles ($\pm 0.5°$) compared with that obtained at sideslip angles of $\pm 5°$.

2. At a Mach number of 0.80 the stability derivative C_{n_β} for the complete airplane was approximately constant through the angle-of-attack range. At higher speeds, although having a greater initial value, C_{n_β} decreased with angle of attack (but did not fall below the M = 0.80 level in the range of these tests). This was associated with corresponding reductions with angle of attack of both the total vertical-tail contribution and the load on the exposed part of the vertical tail.

3. The loads on the exposed vertical tail represented between 60 and 80 percent of the total tail contribution to side force, being greatest at the highest angle of attack where the carryover to the fuselage was reduced.

4. The center of pressure of the exposed vertical tail moved upward and rearward with both angle of attack and Mach number. Maximum movement was approximately 7 percent of the height and 14 percent of the local chord.

5. The use of a wing pitching-moment fix of the drooped chord-extension type extended the linear portion of the C_{l_β} curve to higher angles of attack and reduced the severity of the positive breaks.

6. The pitching-moment-coefficient increment for a sideslip angle of 5° was less than -0.005 for zero angle of attack, but was as much as -0.015 for higher angles of attack.

Langley Aeronautical Laboratory,
National Advisory Committee for Aeronautics,
Langley Field, Va., November 30, 1955.

REFERENCES

1. Zimmerman, Charles H.: Recent Stability and Aerodynamic Problems and Their Implications as to Load Estimation. NACA RM L55E11a, 1955.

2. Kuhn, Richard E., Hallissy, Joseph M., Jr., and Stone, Ralph W., Jr.: A Discussion of Recent Wind-Tunnel Studies Relating to the Problem of Estimating Vertical- and Horizontal-Tail Loads. NACA RM L55E16a, 1955.

3. Runckel, Jack F., and Schmeer, James W.: The Aerodynamic Characteristics at Transonic Speeds of a Model With a 45° Sweptback Wing, Including the Effect of Leading-Edge Slats and a Low Horizontal Tail. NACA RM L53J08, 1954.

4. Whitcomb, Charles F., and Norton, Harry T., Jr.: Transonic Investigation of Aerodynamic Characteristics of a Swept-Wing Fighter-Airplane Model With Leading-Edge Droop in Combination With Outboard Chord-Extensions and Notches. NACA RM L55H30, 1956.

5. Whitcomb, Charles F., and Lee, Edwin E., Jr.: Drag Investigation of a Swept-Wing Fighter-Airplane Model Incorporating Two Drag-Rise-Reducing Fuselage Revisions. NACA RM L55E24, 1955.

6. Osborne, Robert S., and Mugler, John P., Jr.: Aerodynamic Characteristics of a 45° Sweptback Wing-Fuselage Combination and the Fuselage Alone Obtained in the Langley 8-Foot Transonic Tunnel. NACA RM L52E14, 1952.

7. Polhamus, Edward C., and Sleeman, William C., Jr.: The Rolling-Moment Due to Sideslip of Swept Wings at Subsonic and Transonic Speeds. NACA RM L54L01, 1955.

8. Wiley, Harleth G., and Moseley, William C., Jr.: An Investigation at High Subsonic Speeds of the Effects of Horizontal-Tail Height on the Aerodynamic and Loading Characteristics in Sideslip on a 45° Sweptback, Untapered Tail Assembly As Determined From Force Tests and Integrated Vertical-Tail Span Loadings. NACA RM L55E04, 1955.

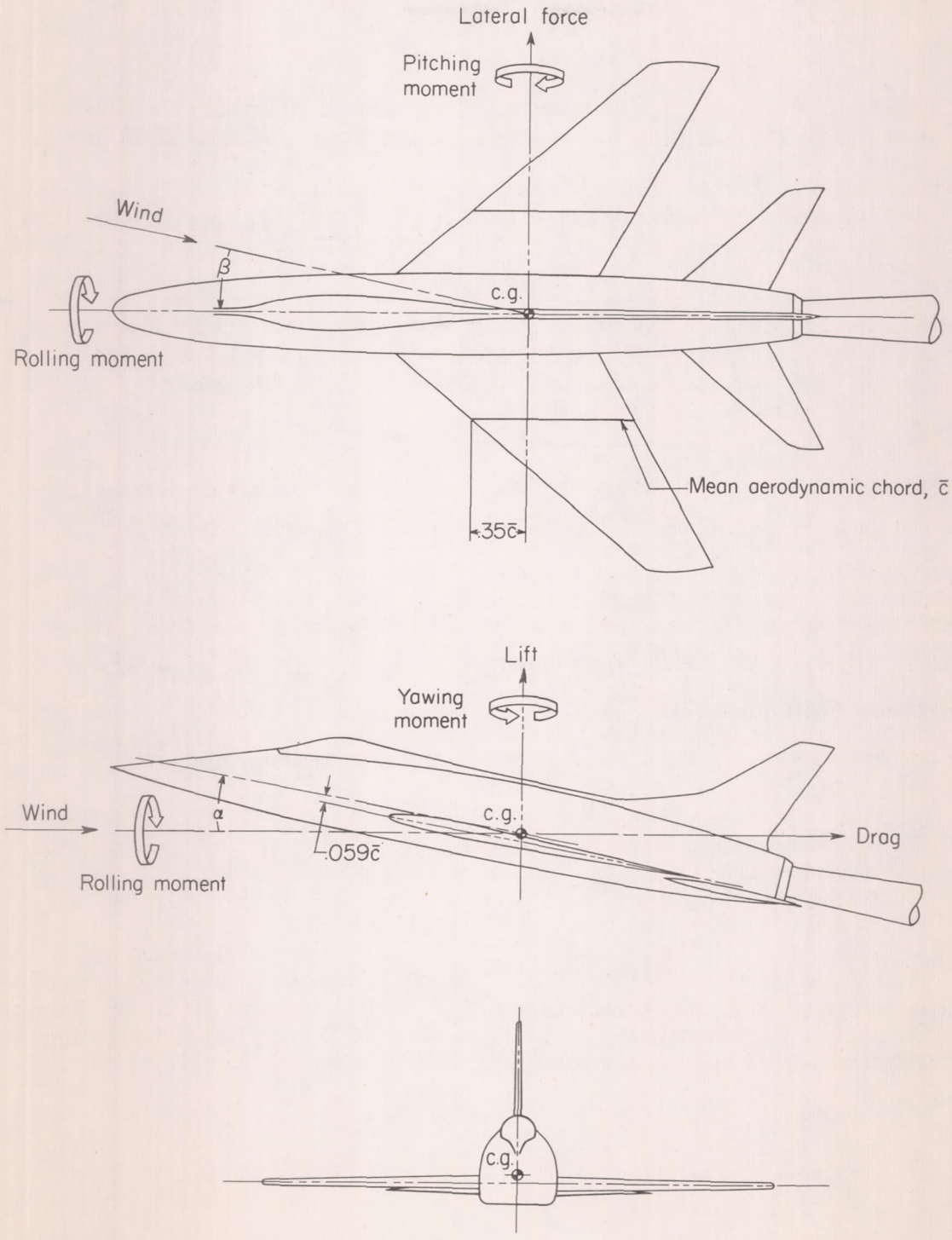

Figure 1.- Sketch of the wind-tunnel model showing the center-of-gravity location and stability-axes system used in reducing data for this report. The positive direction of forces, moments, and angles is indicated by the arrows.

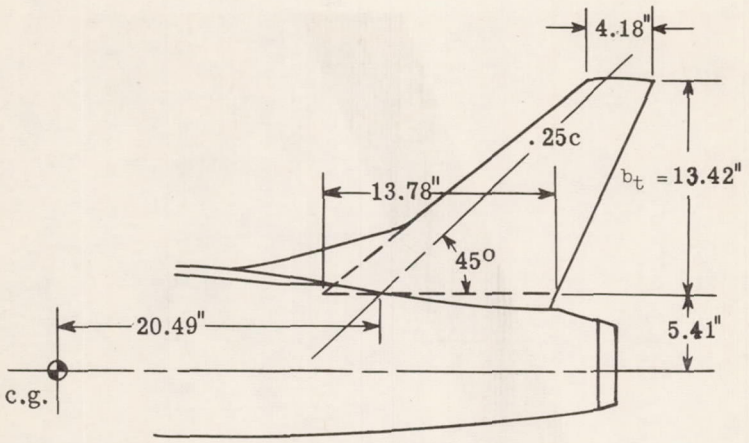

Vertical tail

Sweep at the quarter chord, deg	45
Aspect ratio	1.49
Taper ratio	0.30
Section	NACA 64A007
Area (exposed part less dorsal), sq ft	0.895
Dorsal area, sq ft	0.083

Horizontal tail

Sweep at the quarter chord, deg	45
Aspect ratio	3.56
Taper ratio	0.30
Section	NACA 64A007
Span, in.	33.80
Area, sq ft	2.23

Wing

Sweep at the quarter chord, deg	45
Aspect ratio	3.56
Taper ratio	0.30
Section	NACA 64A007
Span, in.	65.84
Mean aerodynamic chord, in.	20.39
Area, sq ft	8.46

Figure 2.- Vertical-tail and other model dimensions.

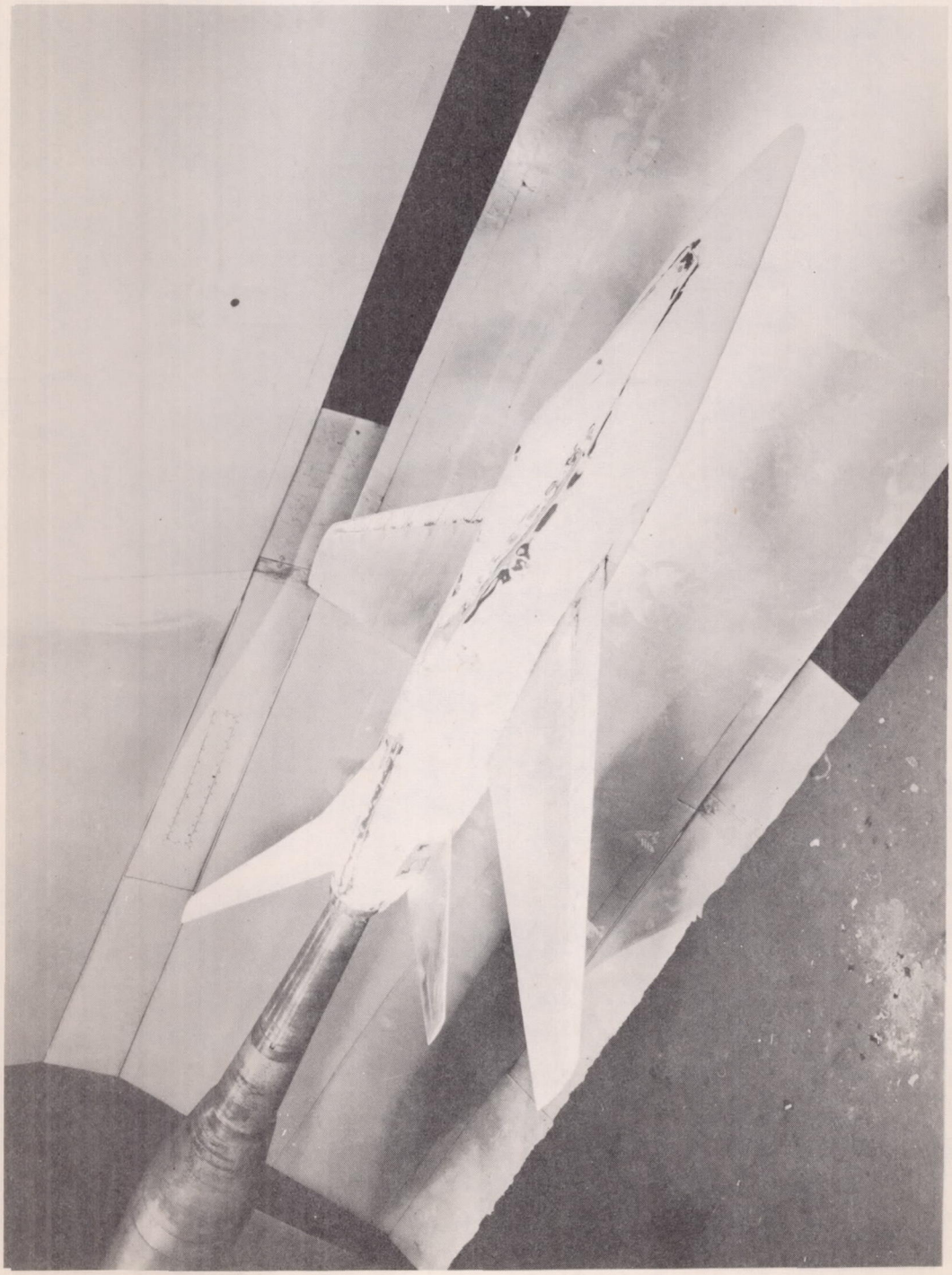

L-82817

Figure 3.- Test model installed in the Langley 16-foot tunnel.

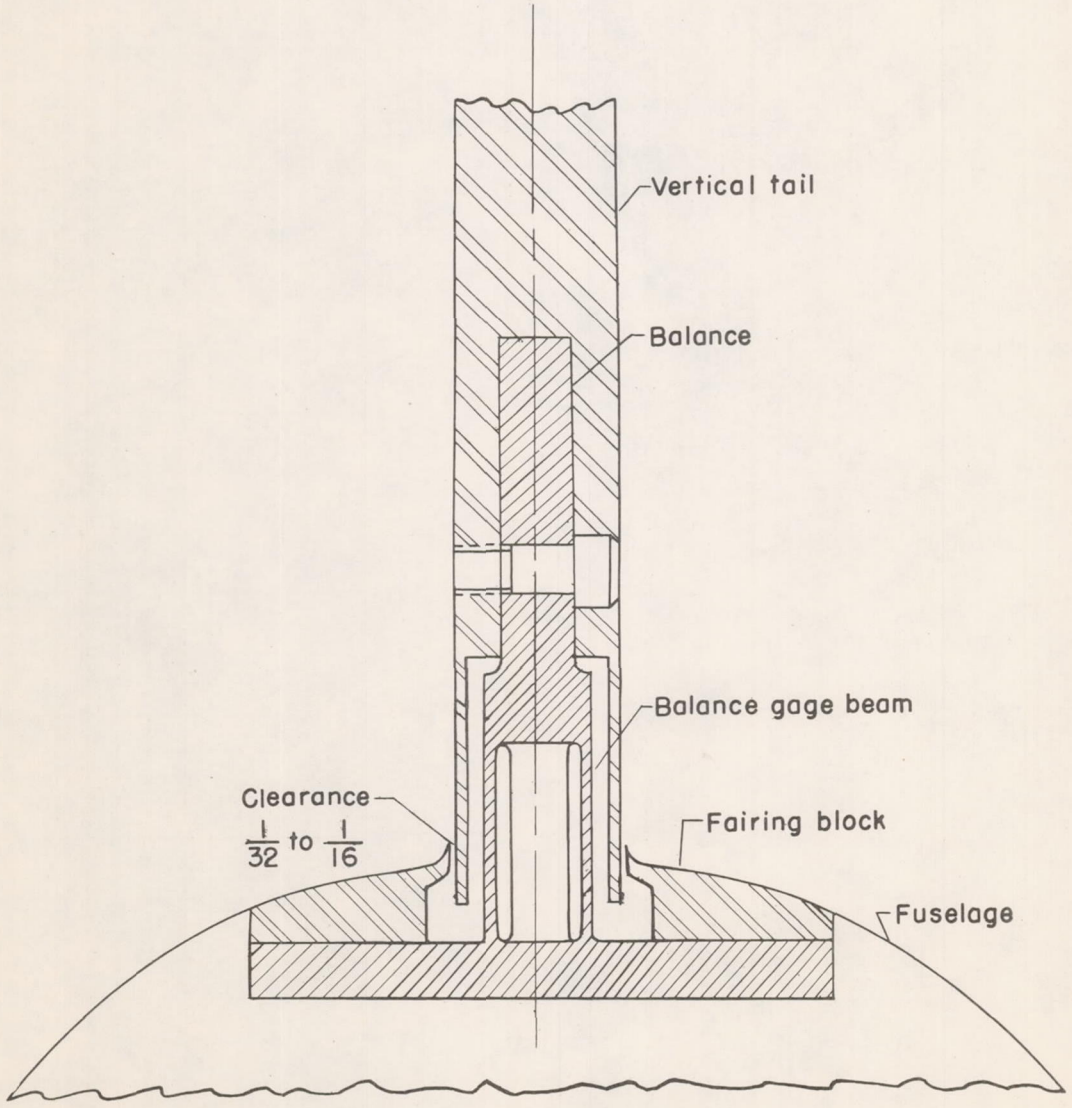

Figure 4.- Typical cross section through instrumented vertical tail.

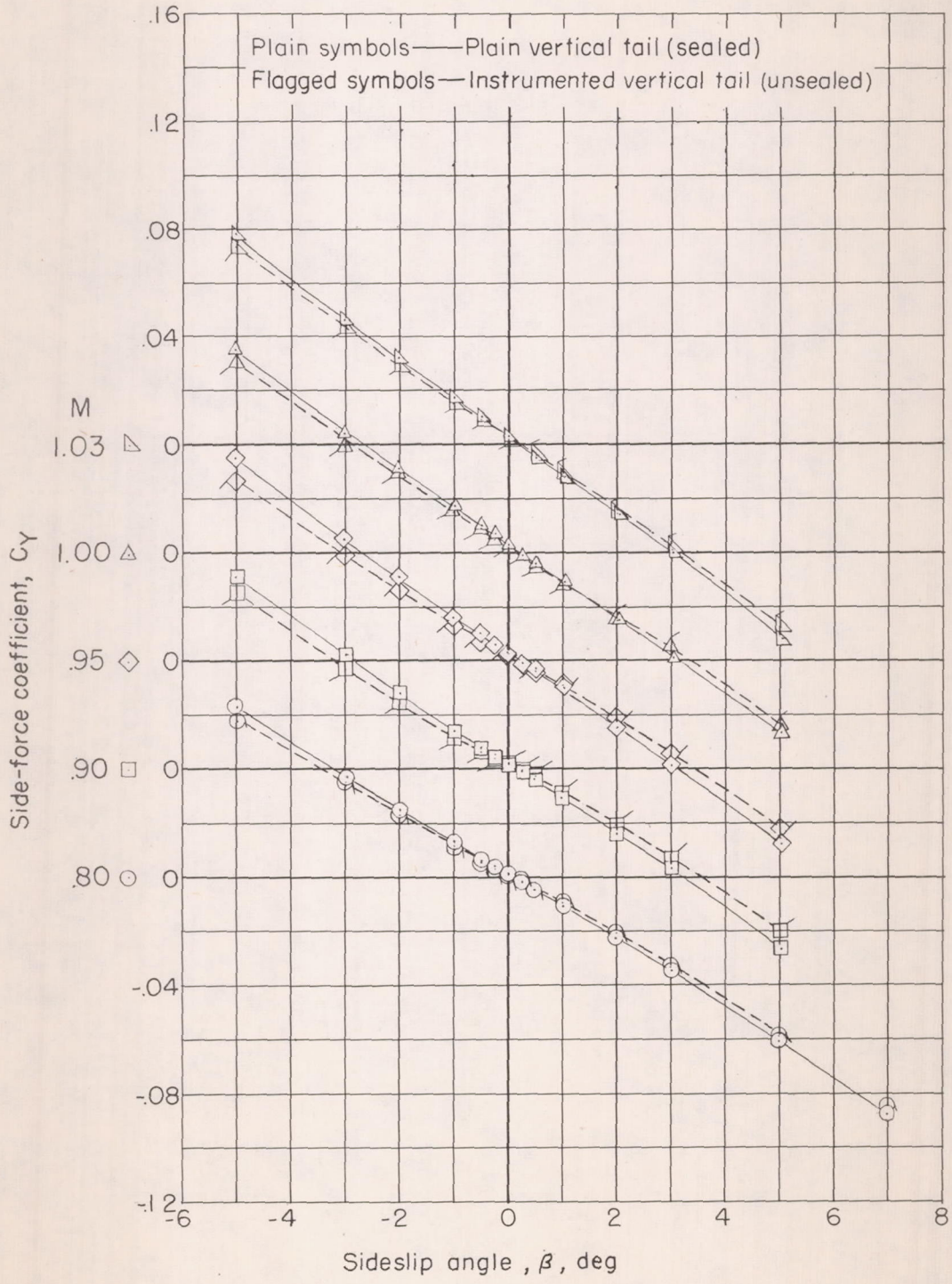

(a) Side force.

Figure 5.- Tail-on variation of lateral airplane coefficients with sideslip at $\alpha = 0^{\circ}$.

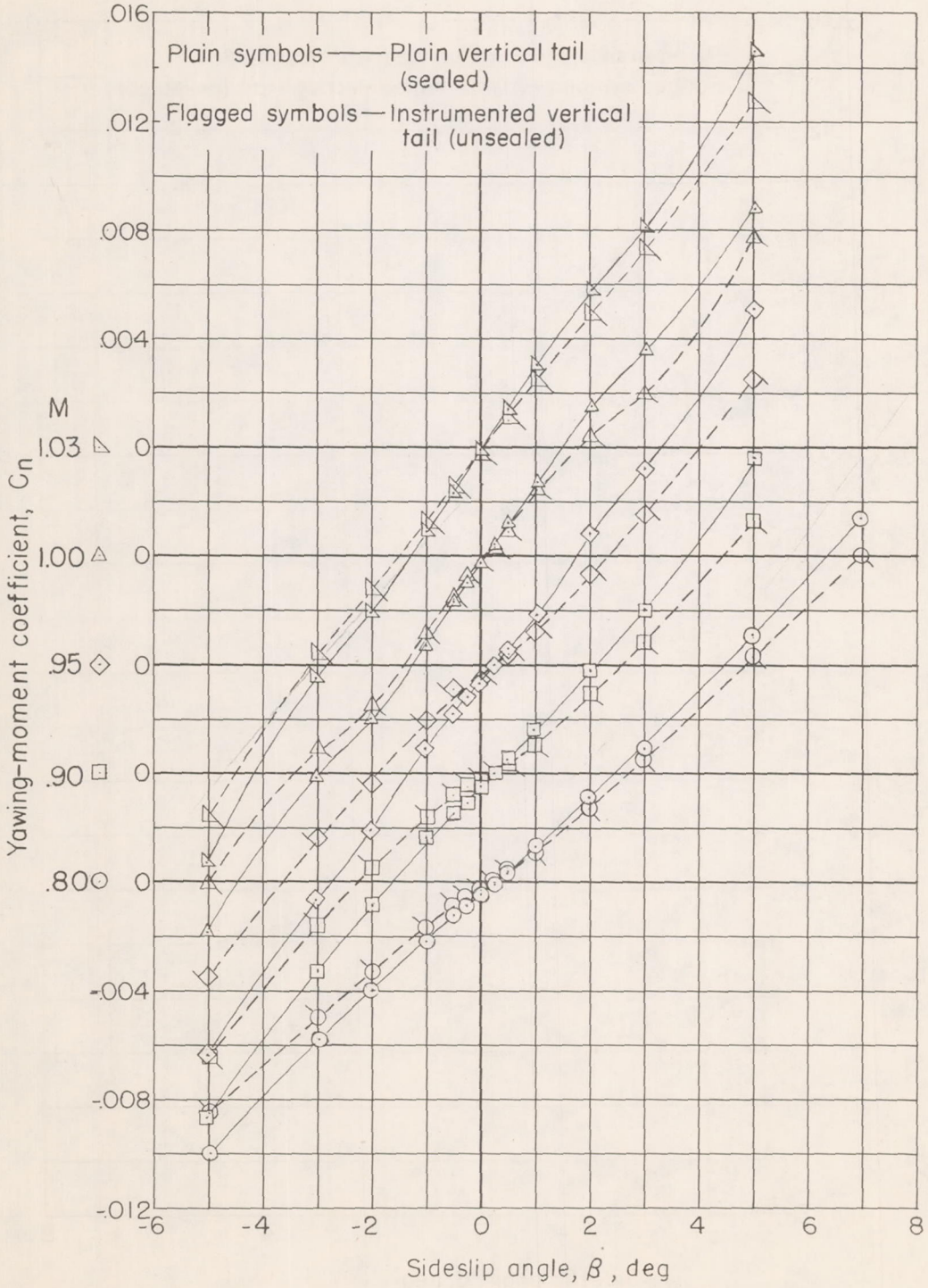

(b) Yawing moment.

Figure 5.- Continued.

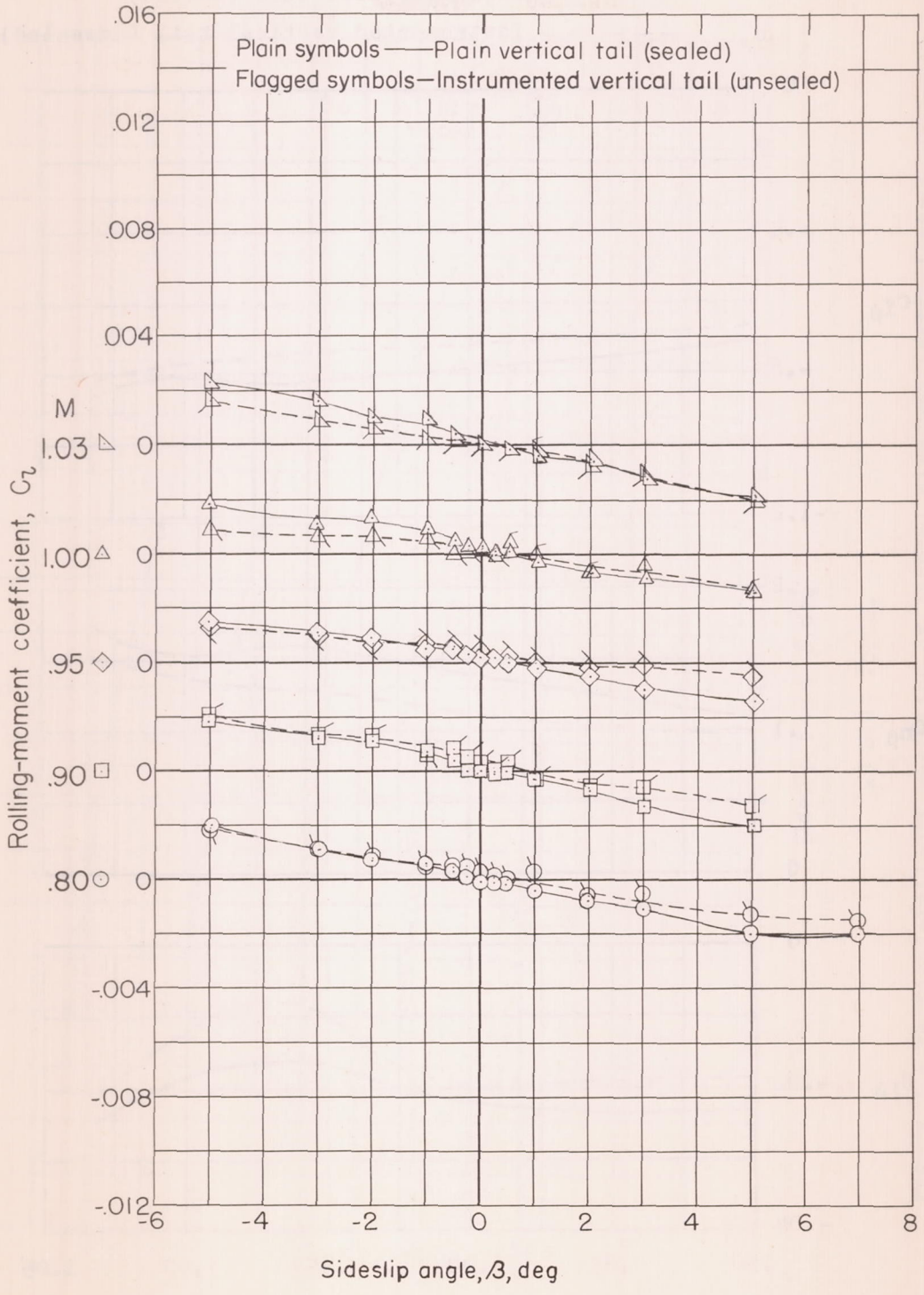

(c) Rolling moment.

Figure 5.- Concluded.

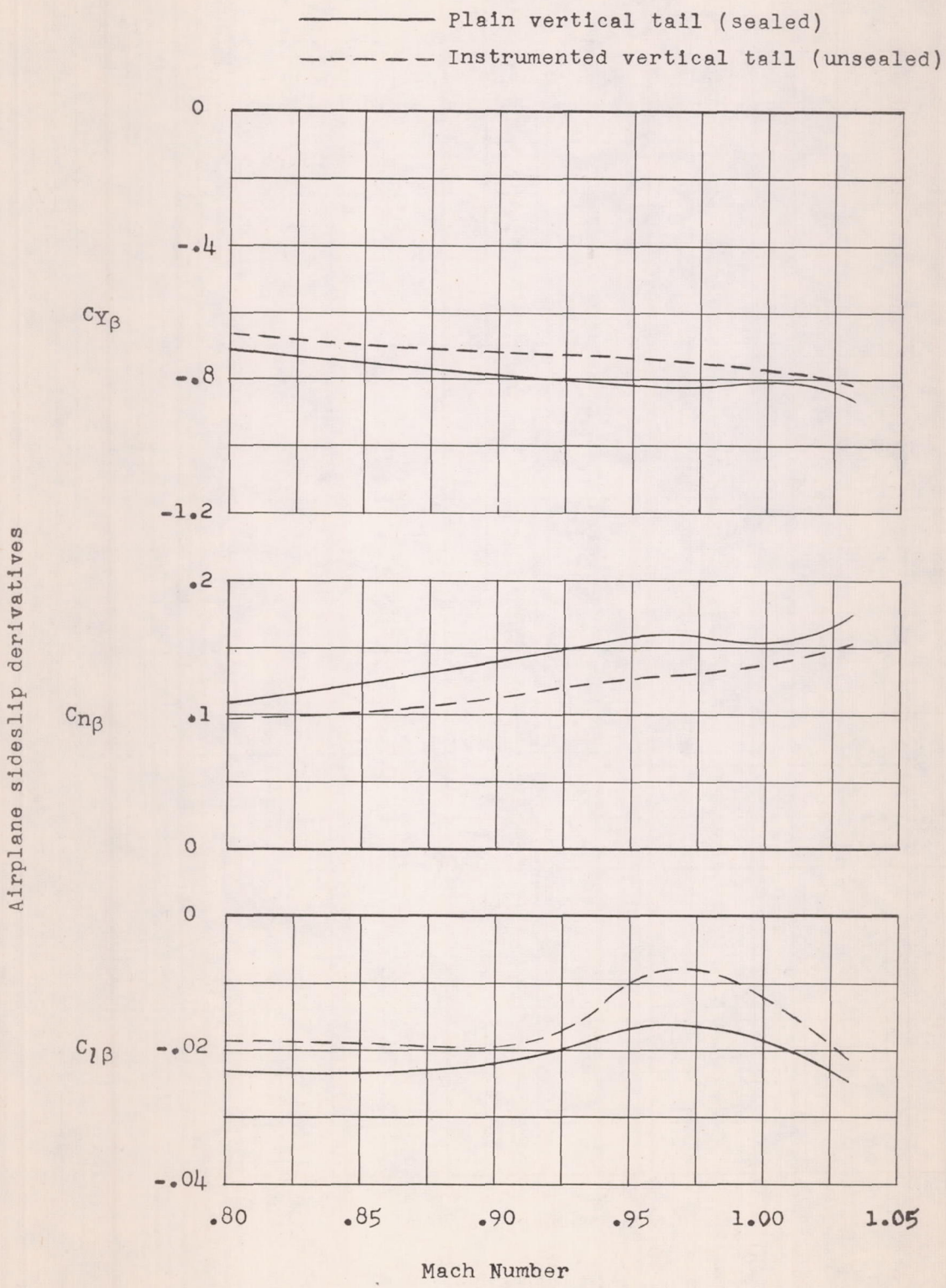

Figure 6.- Effect of unsealed vertical-tail root on the airplane sideslip derivatives. $\alpha = 0^\circ$.

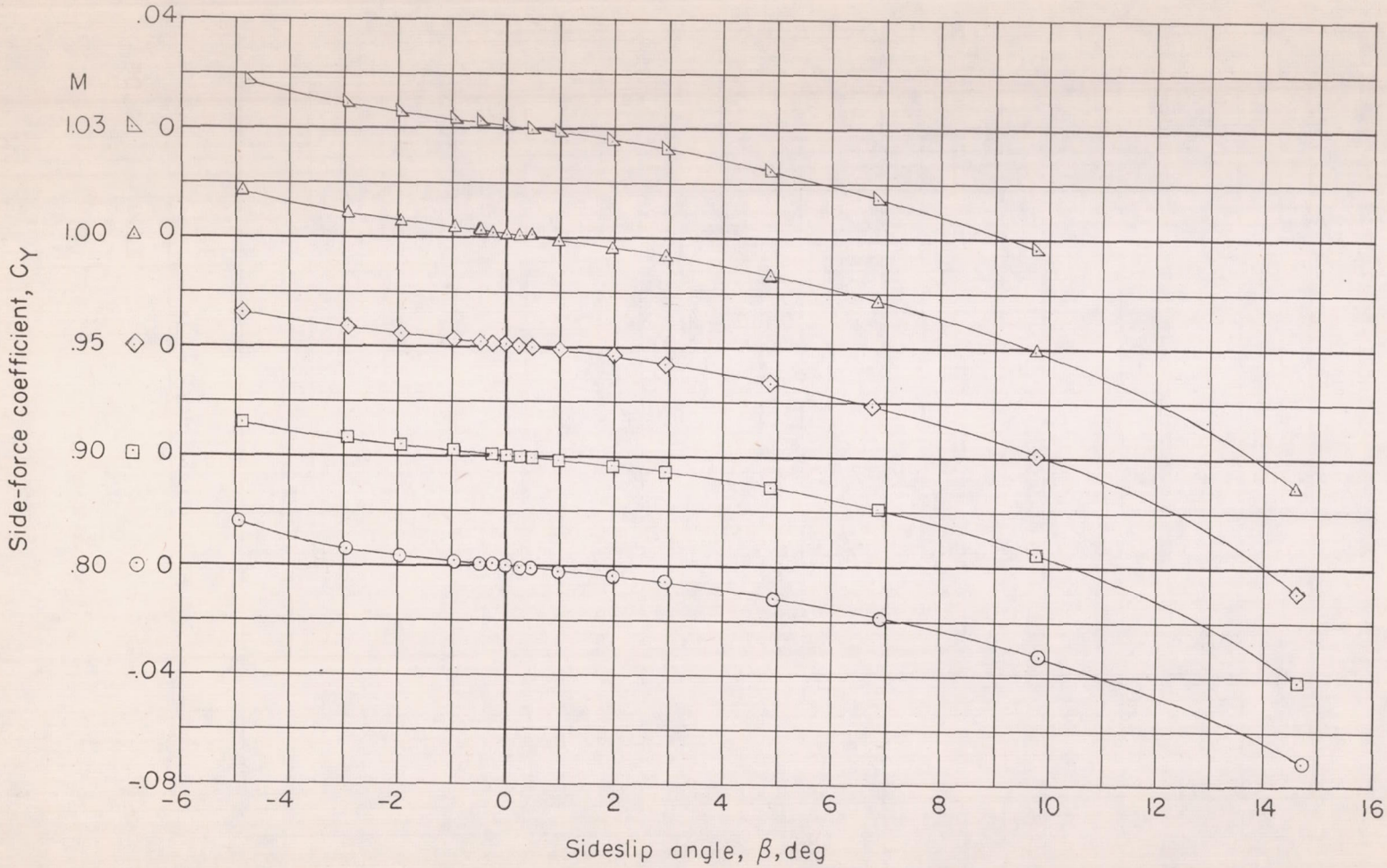

(a) Side force.

Figure 7.- Vertical-tail-off variation of lateral airplane coefficients with sideslip angle at $\alpha = 0^{\circ}$.

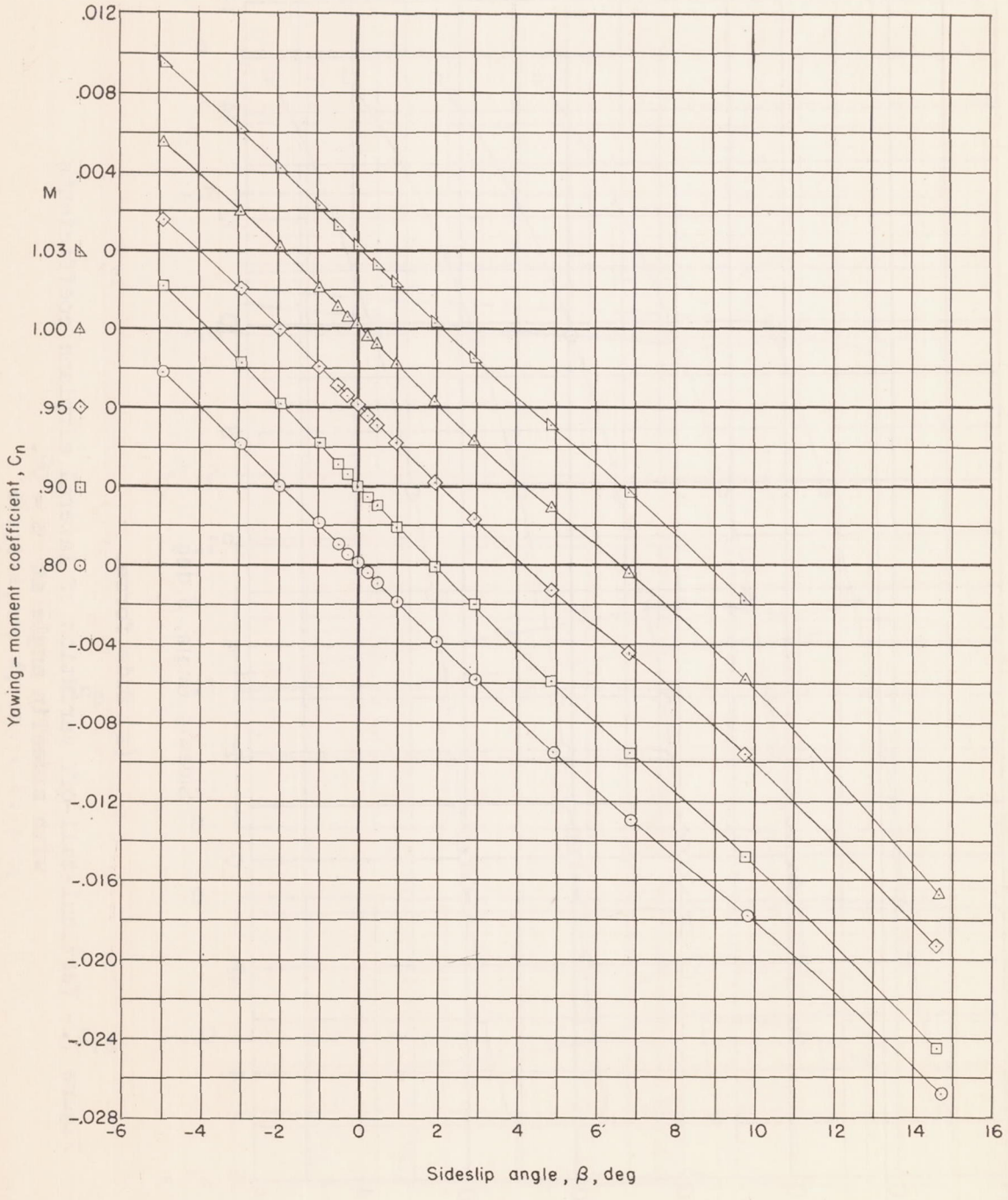

(b) Yawing moment.

Figure 7.- Continued.

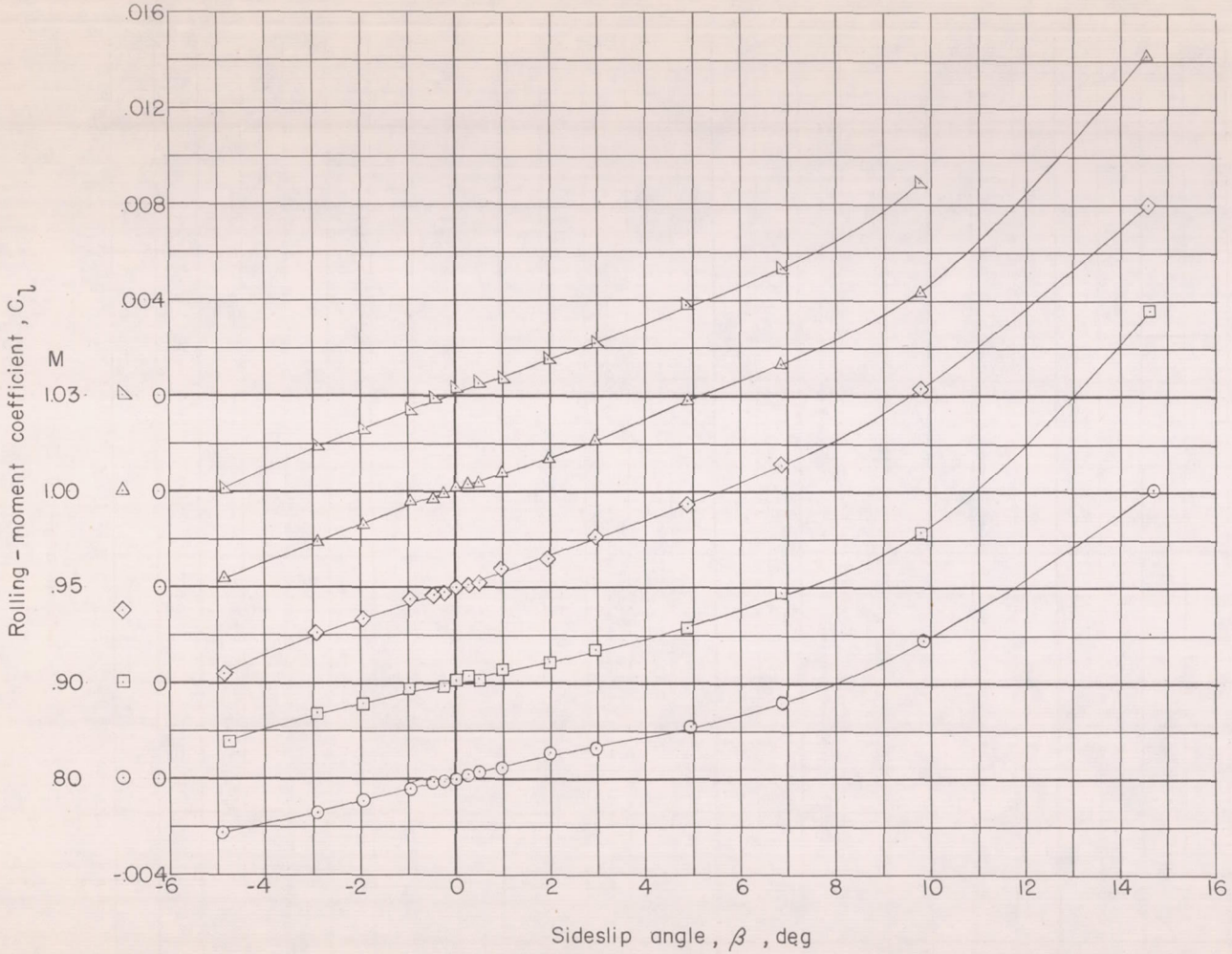

(c) Rolling moment.

Figure 7.- Concluded.

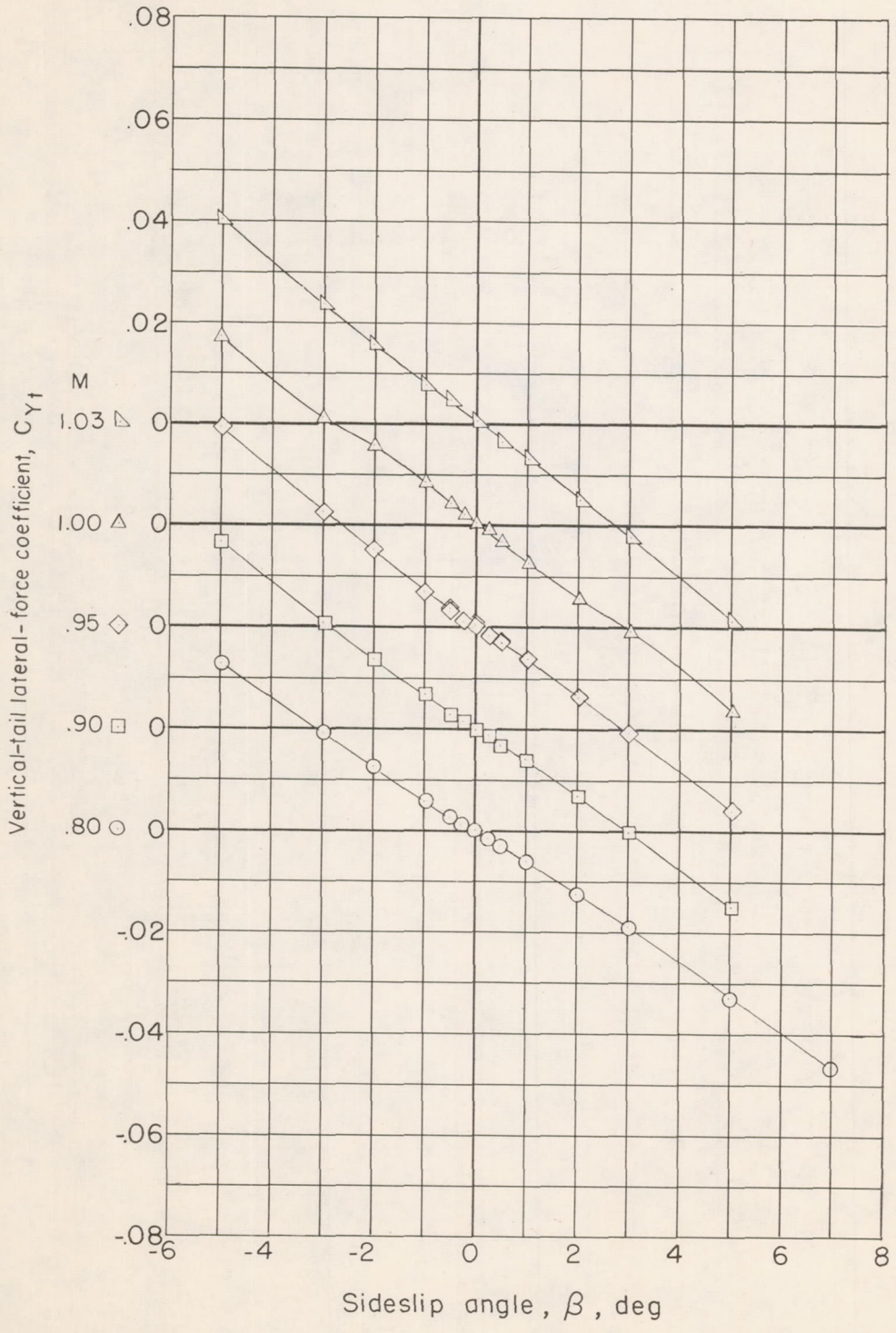

(a) Vertical-tail lateral force.

Figure 8.- Variation of lateral forces and moments with sideslip at $\alpha = 0^\circ$ on the instrumented vertical tail (unsealed).

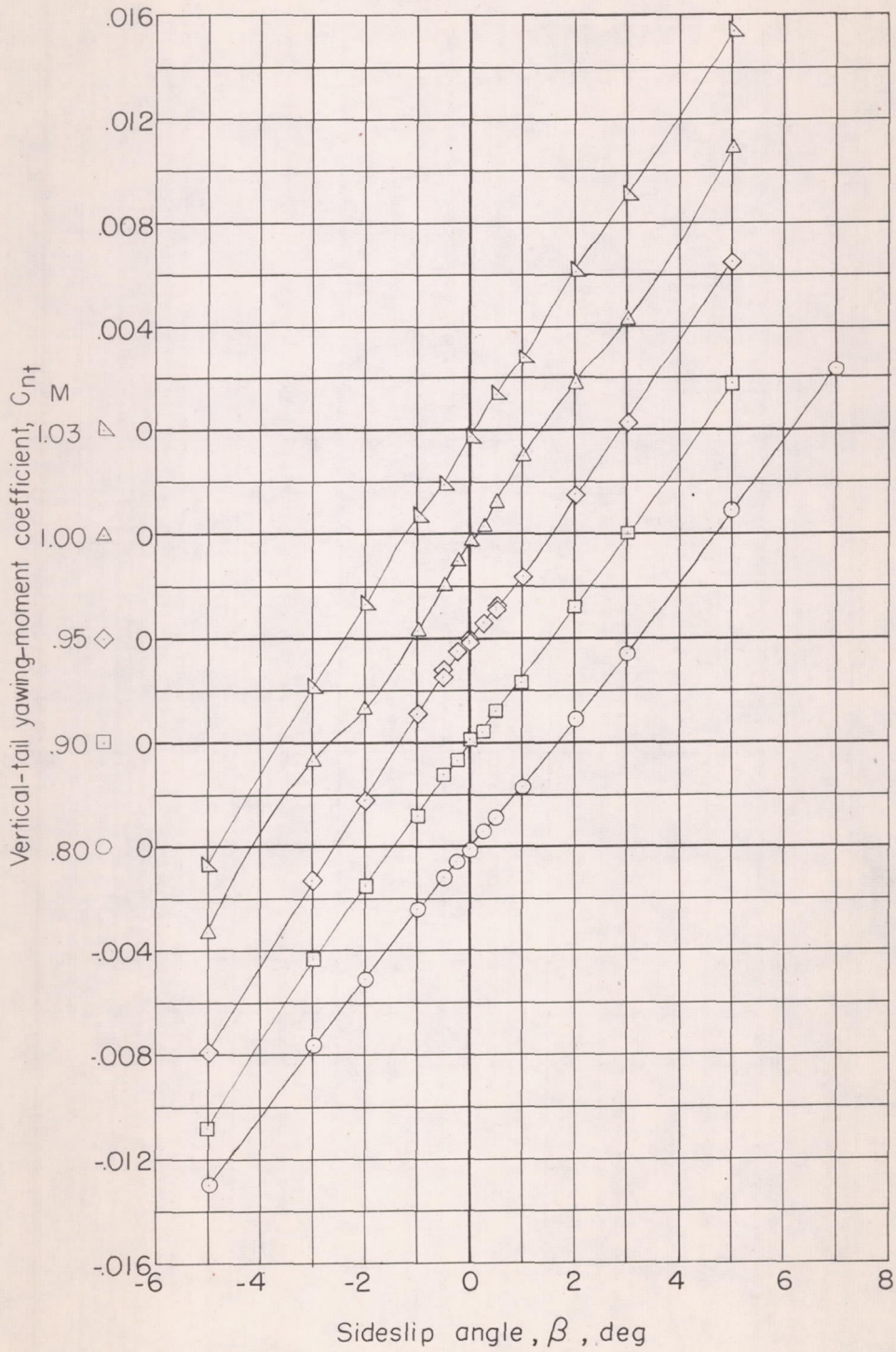

(b) Vertical-tail yawing moment.

Figure 8.- Continued.

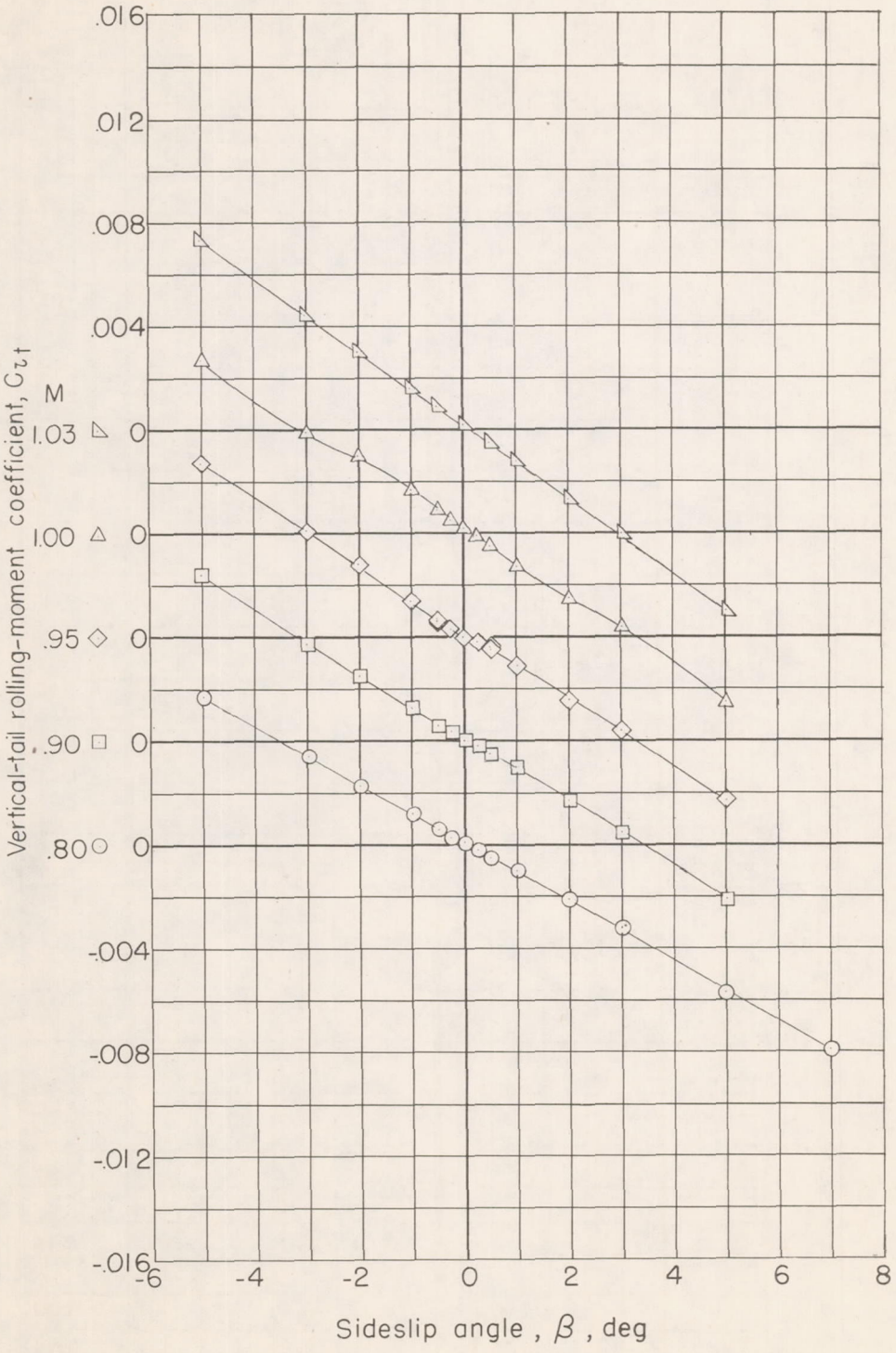

(c) Vertical-tail rolling moment.

Figure 8.- Concluded.

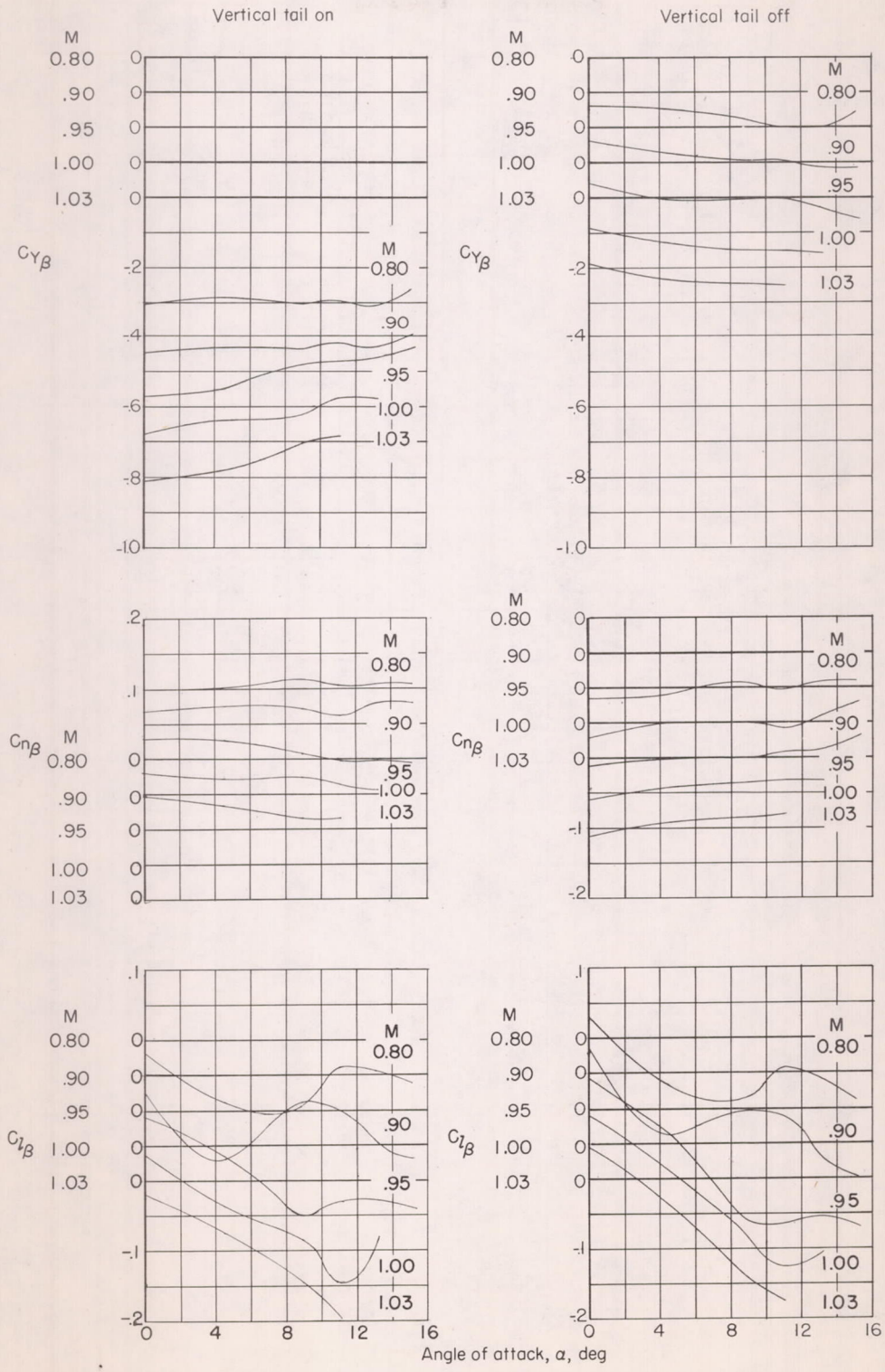

Figure 9.- Variation of sideslip derivatives with angle of attack. Unsealed vertical tail on and off.

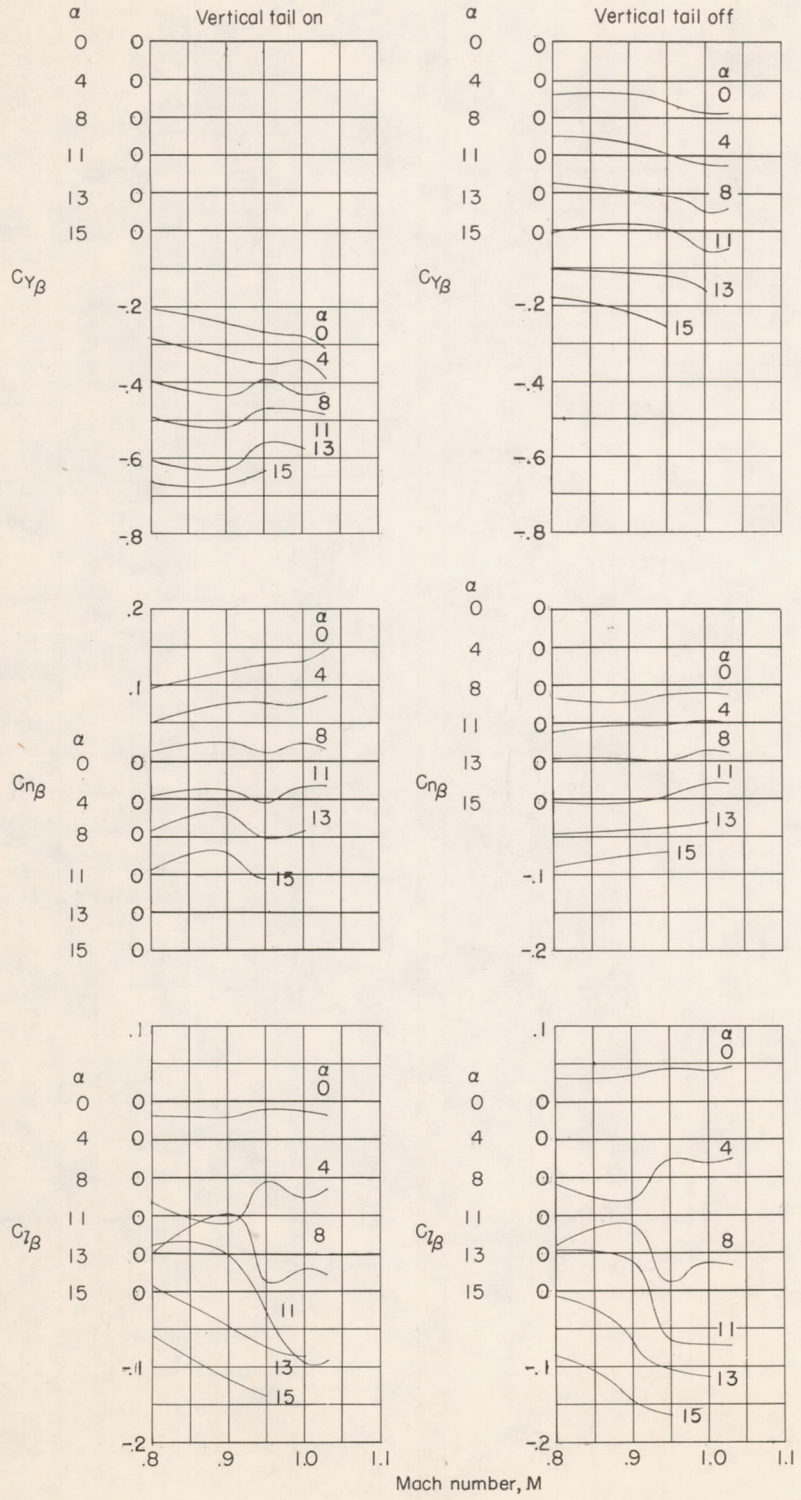

Figure 10.- Variation of sideslip derivatives with Mach number. Unsealed vertical tail on and off.

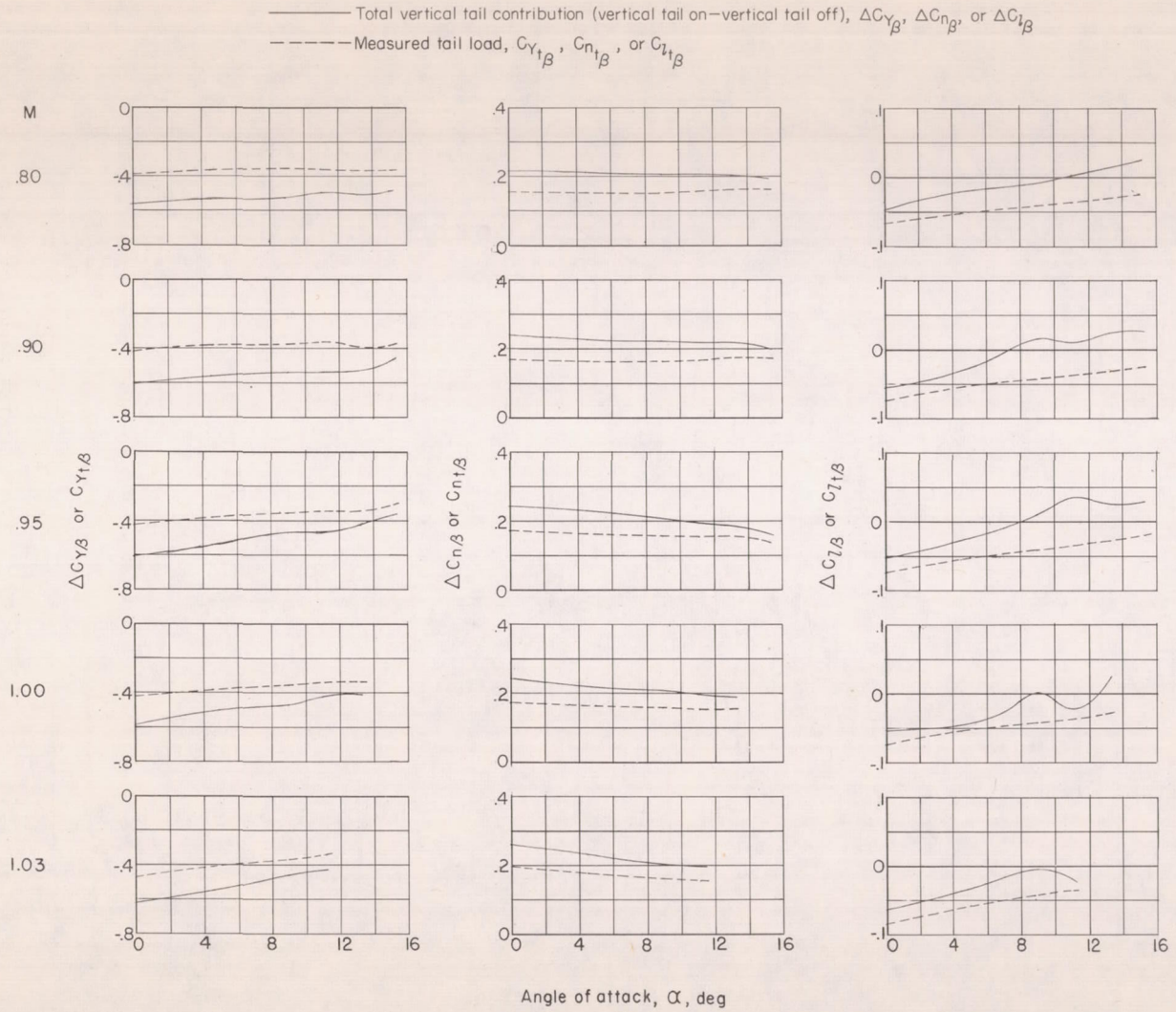

Figure 11.- Variation with angle of attack of unsealed-vertical-tail contribution to the sideslip derivatives.

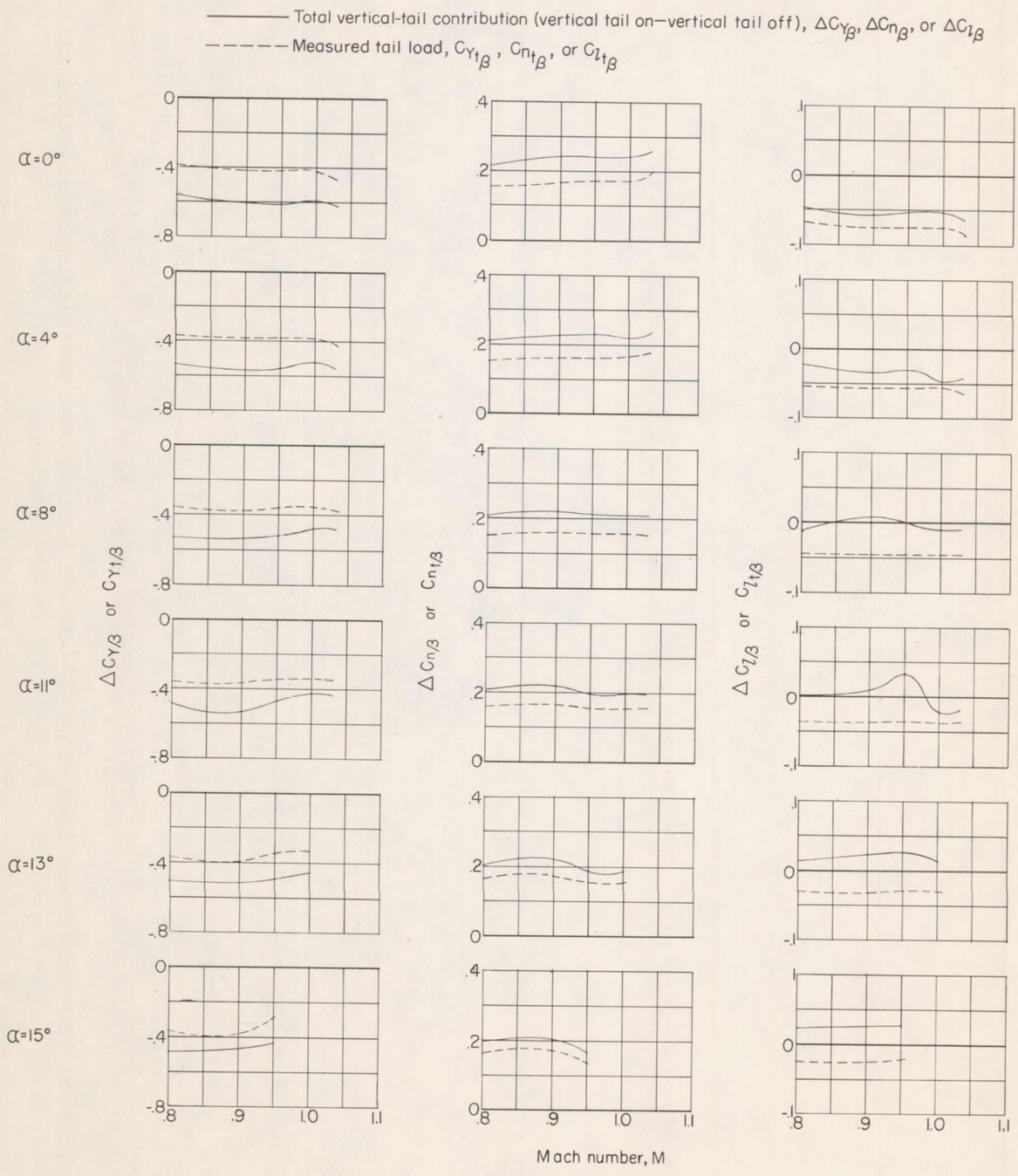

Figure 12.- Variation with Mach number of unsealed-vertical-tail contribution to the sideslip derivatives.

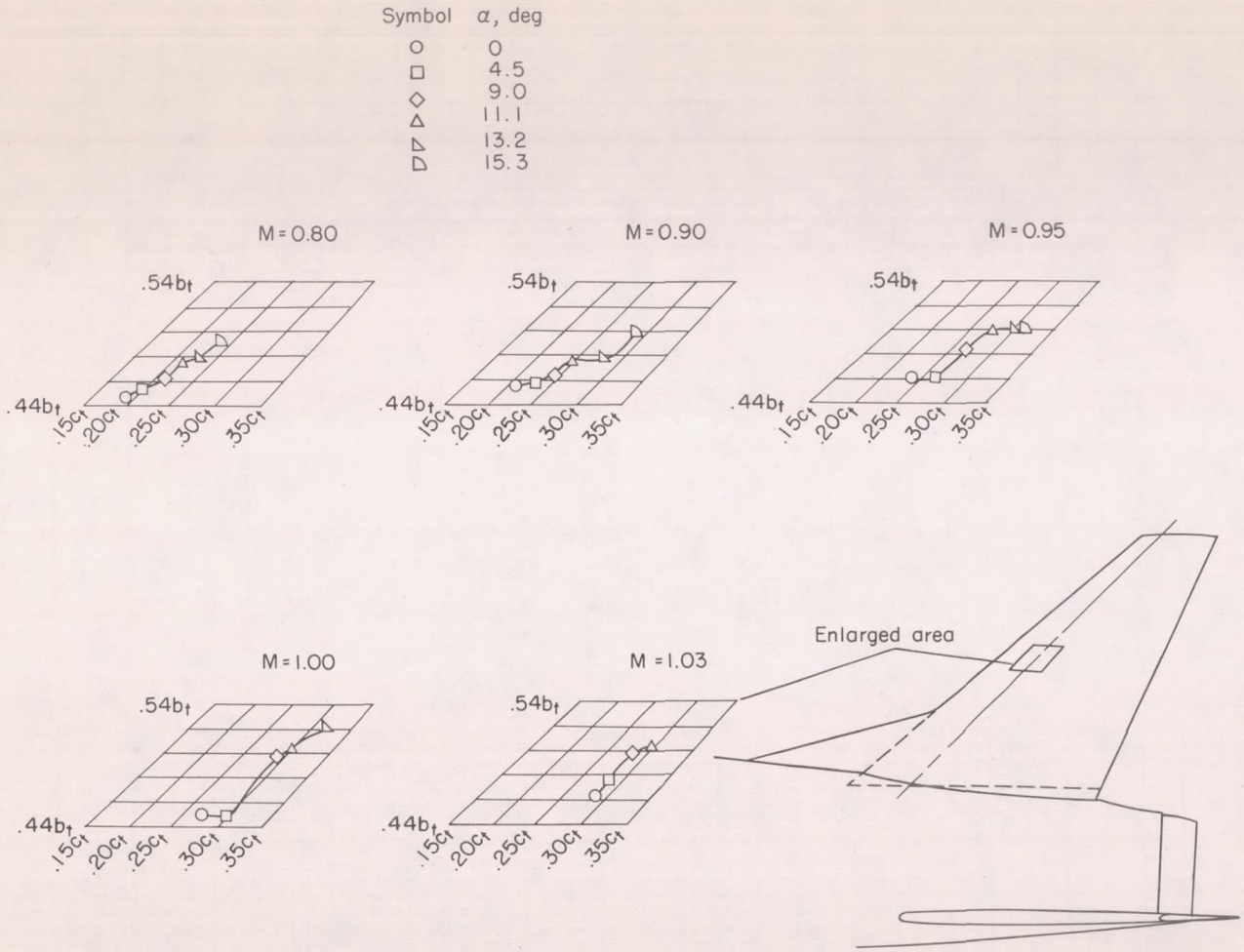

(a) Variation with angle of attack.

Figure 13.- Center-of-pressure locations on the exposed unsealed vertical tail at $\beta = 5^{\circ}$. Basic wing.

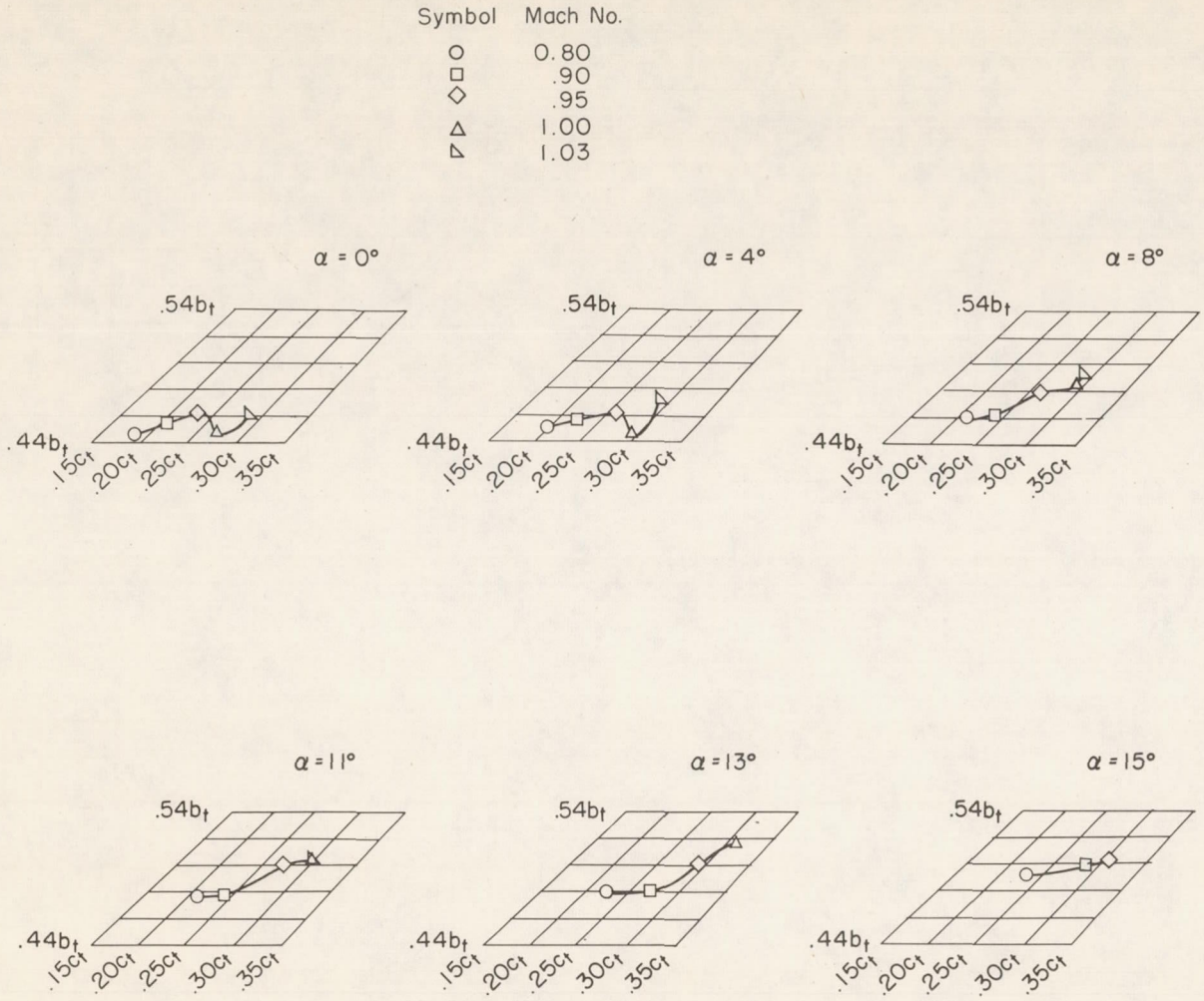

(b) Variation with Mach number.

Figure 13.- Concluded.

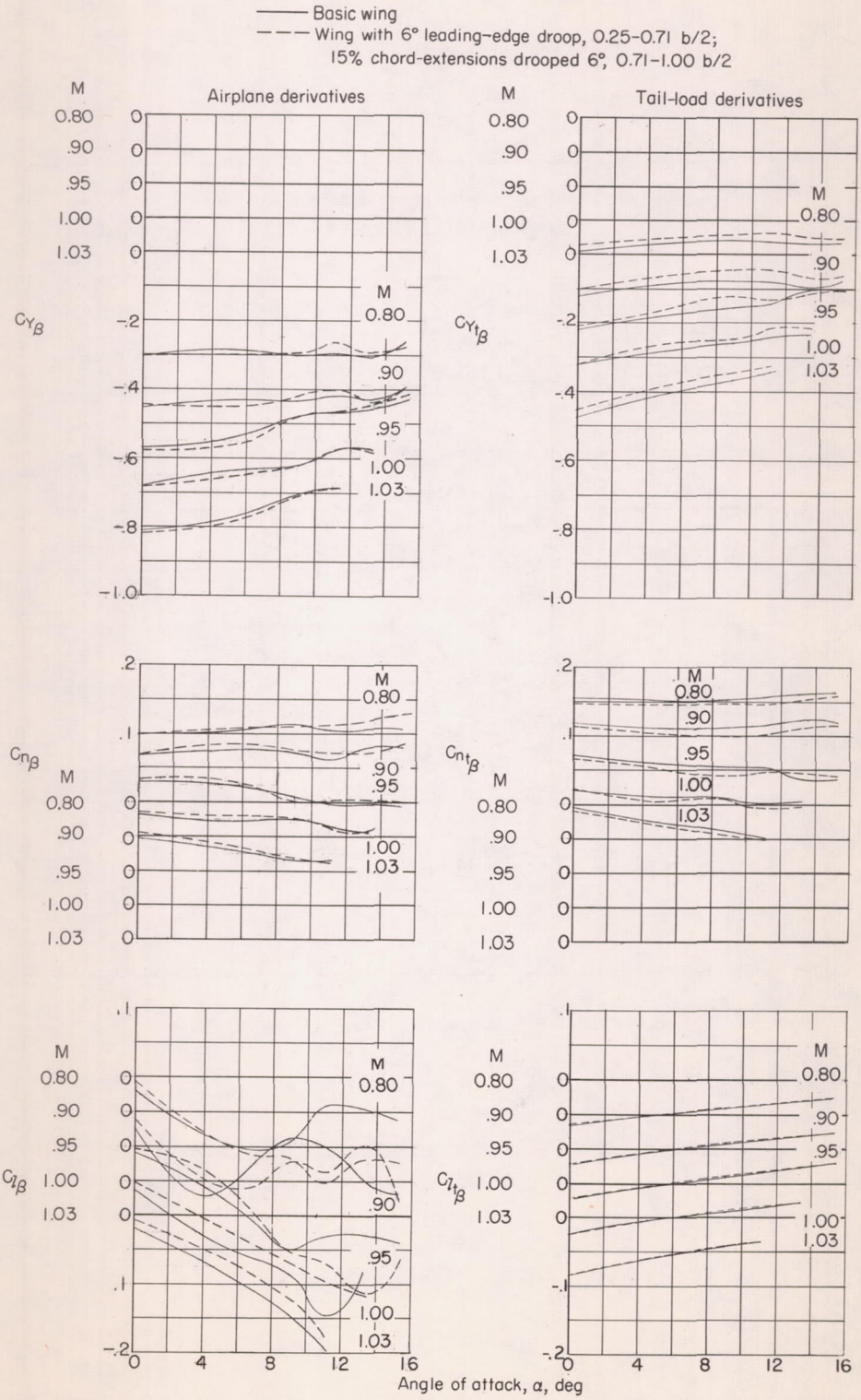

Figure 14.- Effect of leading-edge fix on lateral airplane and tail-load derivatives.

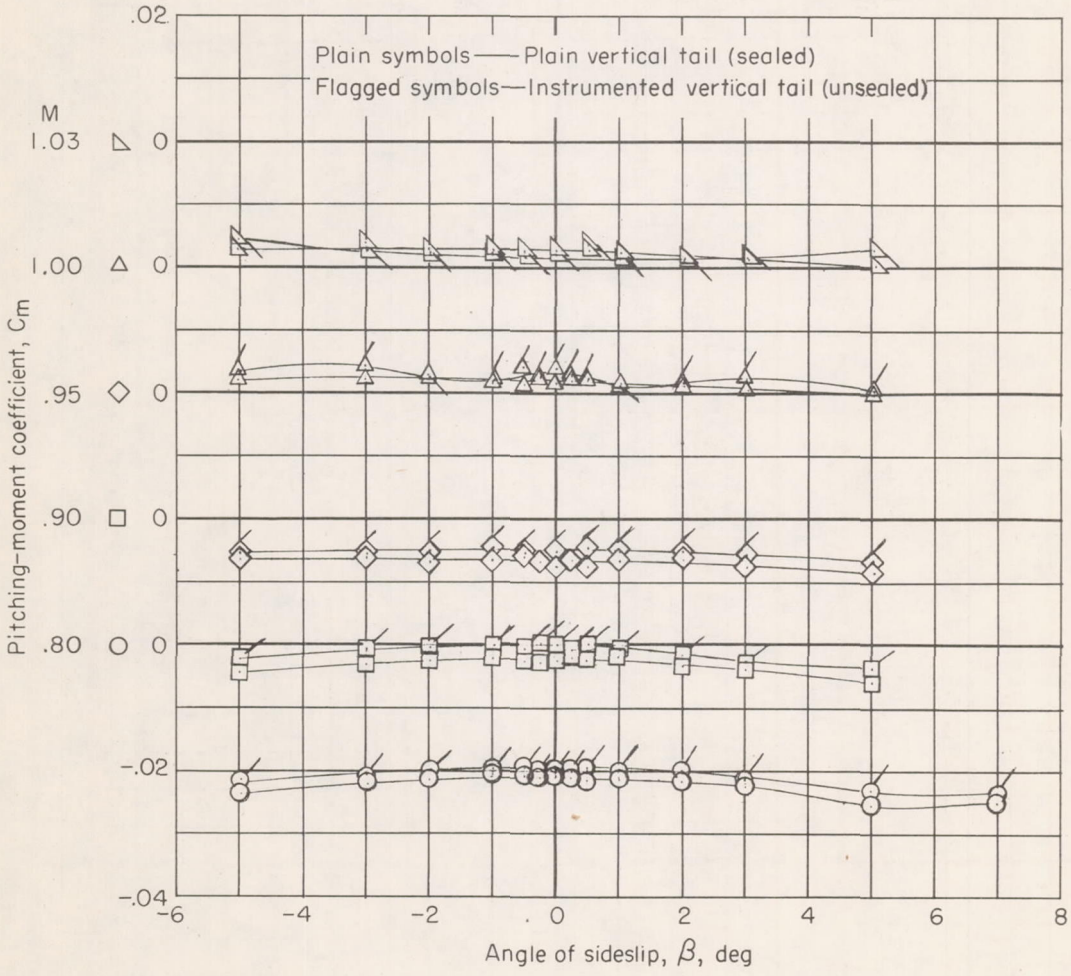

(a) Vertical tail on.

Figure 15.- Variation of pitching-moment coefficient with sideslip at zero angle of attack.

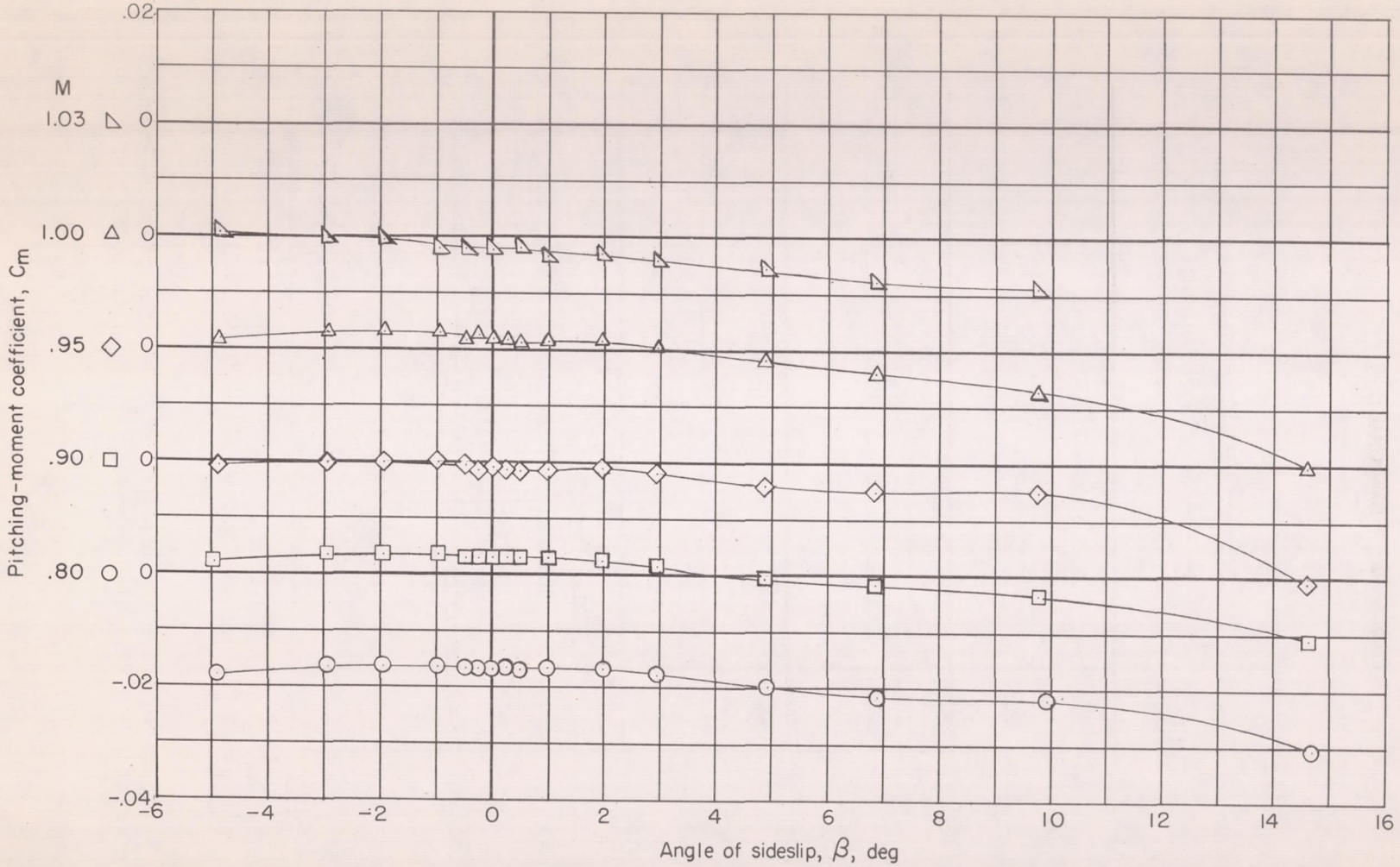

(b) Vertical tail off.

Figure 15.- Concluded.

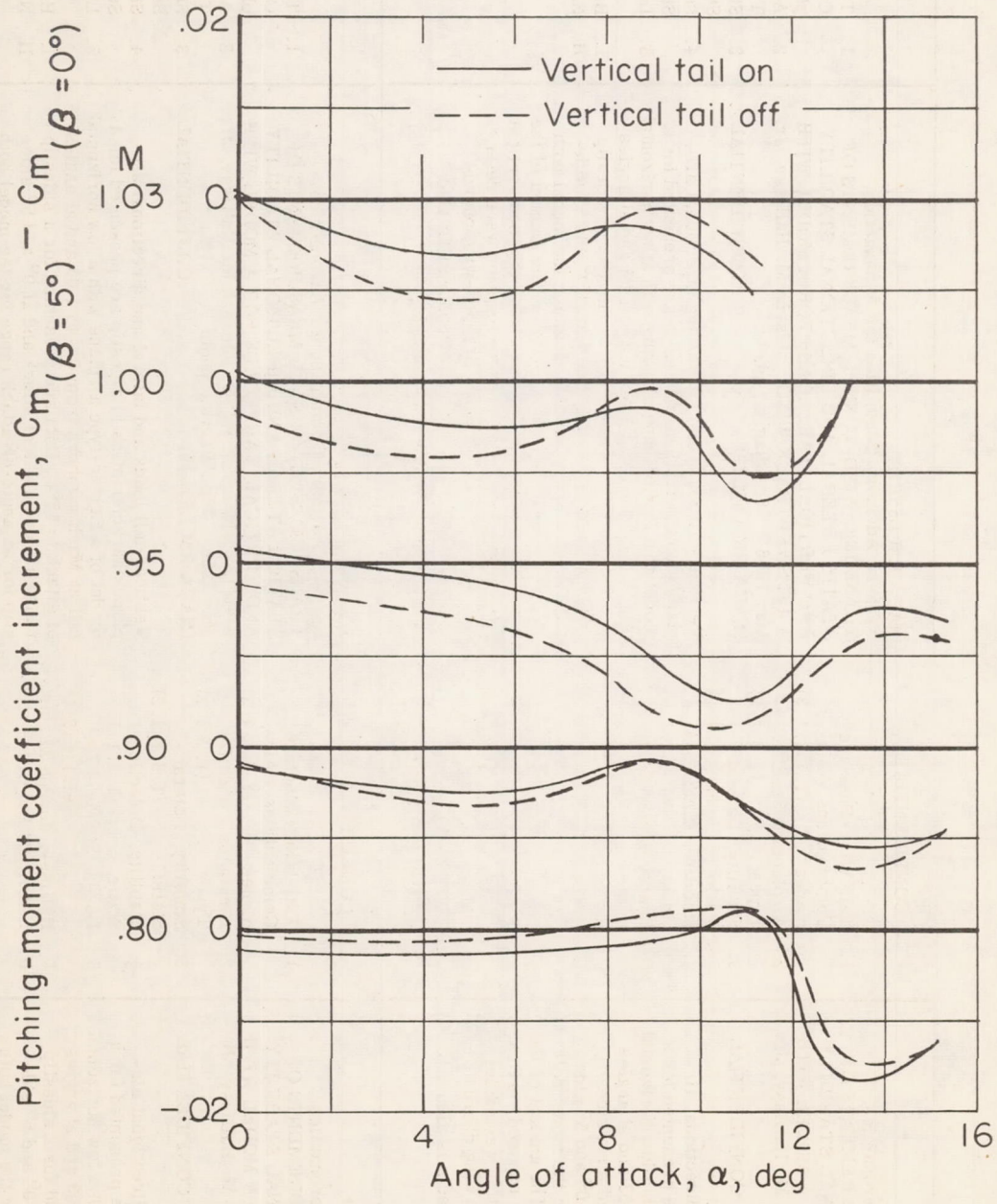

Figure 16.- Effect of a sideslip angle of 5° on the pitching-moment coefficient. Unsealed vertical tail on and off.

NACA - Langley Field, Va.